

Visible-light unmasking of heterocyclic quinone methide radicals from alkoxyamines

Patrick Kielty,^a Pau Farràs,^{a,b} Patrick McArdle,^a Dennis A. Smith^a and Fawaz Aldabbagh^{*,a,c}

^a School of Chemistry, National University of Ireland Galway, University Road, Galway, H91 TK33, Ireland

^b Energy Research Centre, Ryan Institute, National University of Ireland Galway, University Road, Galway, H91 CF50, Ireland

^c Department of Pharmacy, School of Life Sciences, Pharmacy and Chemistry, Kingston University, Penrhyn Road, Kingston upon Thames, KT1 2EE, U.K.

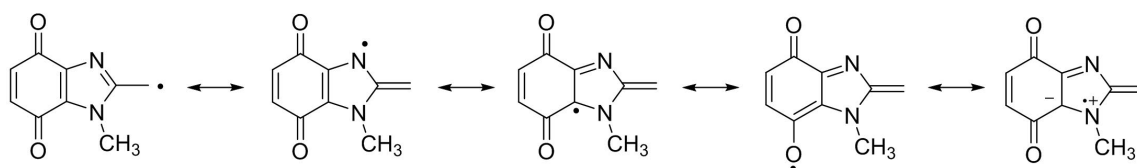
Supplementary Information

Contents

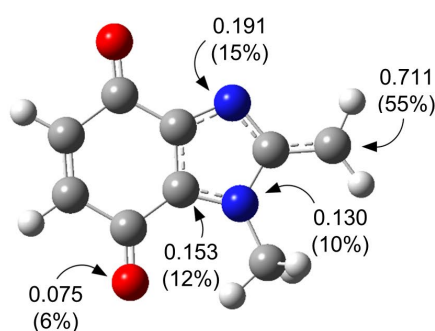
Supporting Figures.....	S3
Supporting Tables	S9
Experimental	S11
Materials.....	S11
Measurements.....	S11
DFT calculations.....	S11
Melting points, ultraviolet-visible and infrared spectroscopy	S12
Nuclear magnetic resonance (NMR spectroscopy)	S12
High resolution mass spectrometry (HRMS)	S12
Single crystal X-ray diffraction	S12
Visible-light photoreactor.....	S13
Analytical HPLC	S13
Homolysis rates (k_d).....	S14
Quantum yield of homolysis (Φ_h).....	S14
Cyclic voltammetry	S14
Synthetic Procedures and Characterization.....	S15
Synthesis of 4,7-dimethoxy-1-methyl-2-[(2,2,6,6-tetramethylpiperidin-1-yl)oxy]methyl}-1 <i>H</i> -benzimidazole (1).....	S15
General procedures (A-C) for the synthesis of benzimidazolequinones via dimethoxybenzimidazole oxidations	S15
References in Supplementary Information	S20
Appendix.....	S21
Tables Referenced in Supplementary Information.....	S21
NMR Spectra.....	S23

Supporting Figures

(A)



(B)



(C)

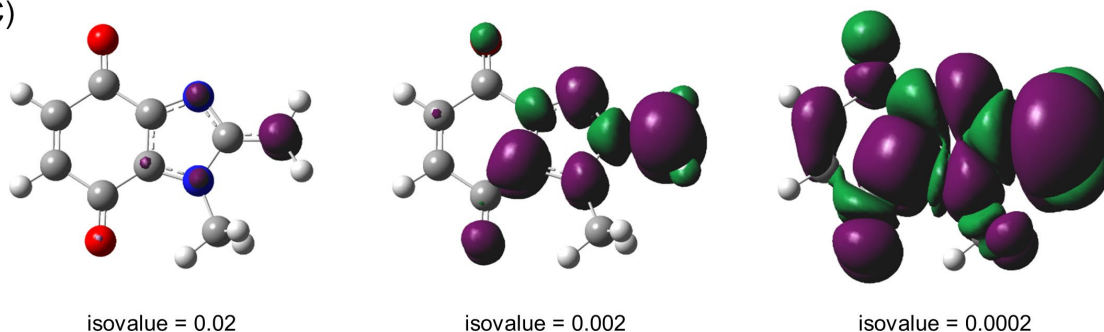


Figure S1 (A) Resonance structures for **QM-rad**; (B) DFT-derived atomic NBO spin densities (the largest positive spin density (α) resides on the exocyclic C-atom (55%), as is typical of a benzylic-type system¹); (C) Spin density distribution across **QM-rad** for three different isovalues with positive spin density appearing in purple and negative spin density in green. Isovalue = 0.002 appears in Scheme 1. Geometry optimization performed in the gas phase using UM06-2X/6-311++G (d,p), and NBO energy calculation performed using UM06-2X/cc-pVTZ.

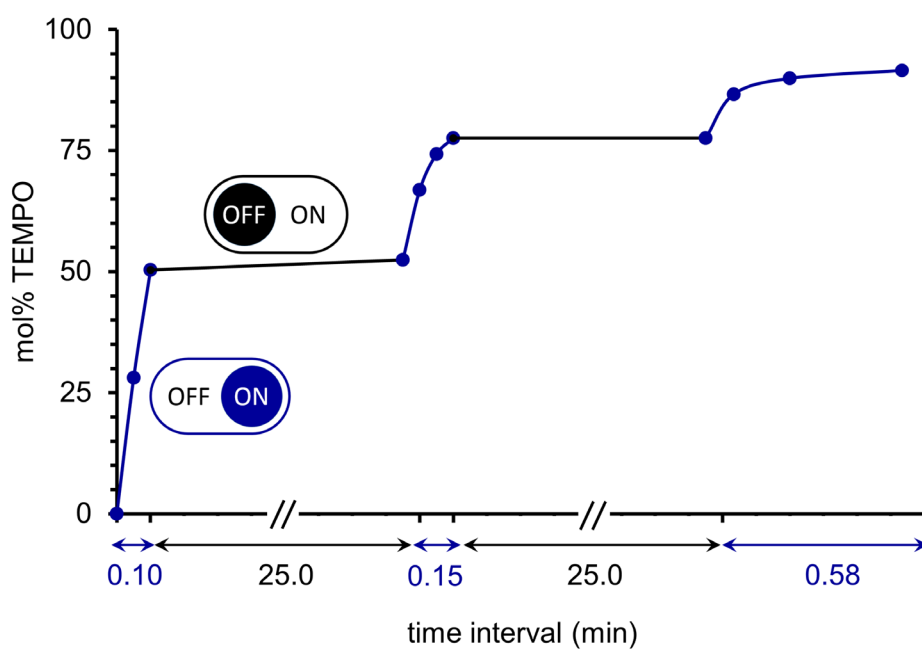
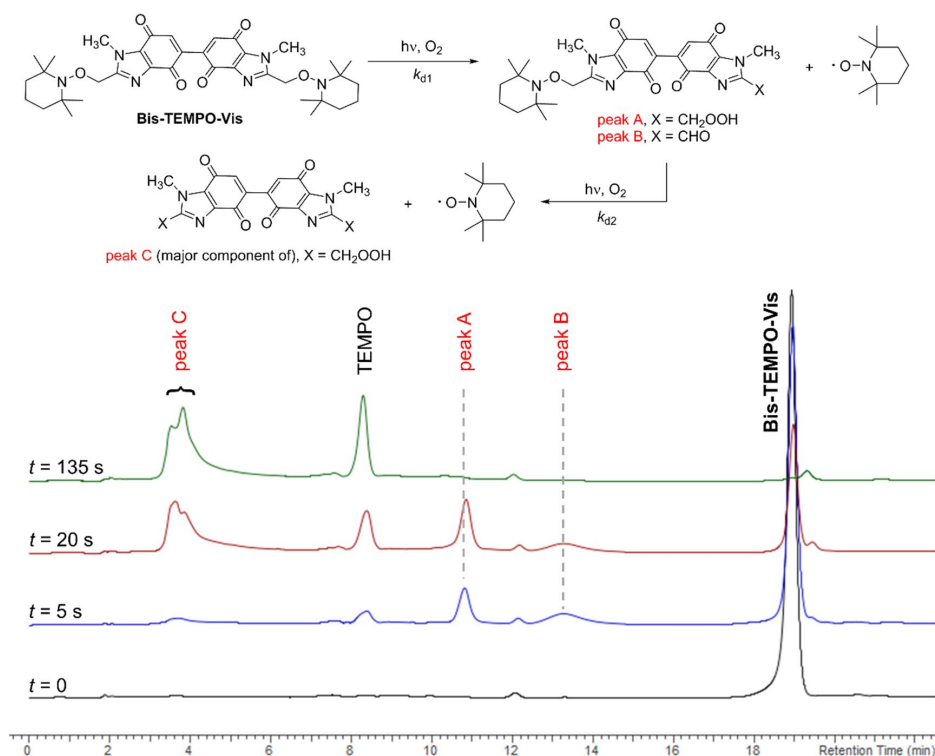


Figure S2 On/off control in the blue LED-induced homolysis of **TEMPO-Vis**. Conditions: **TEMPO-Vis** (0.25 mM, DCE) illuminated by one blue LED bulb (9 W) under O₂ balloon, with HPLC analysis. Connecting lines drawn between data points.

(A)



(B)

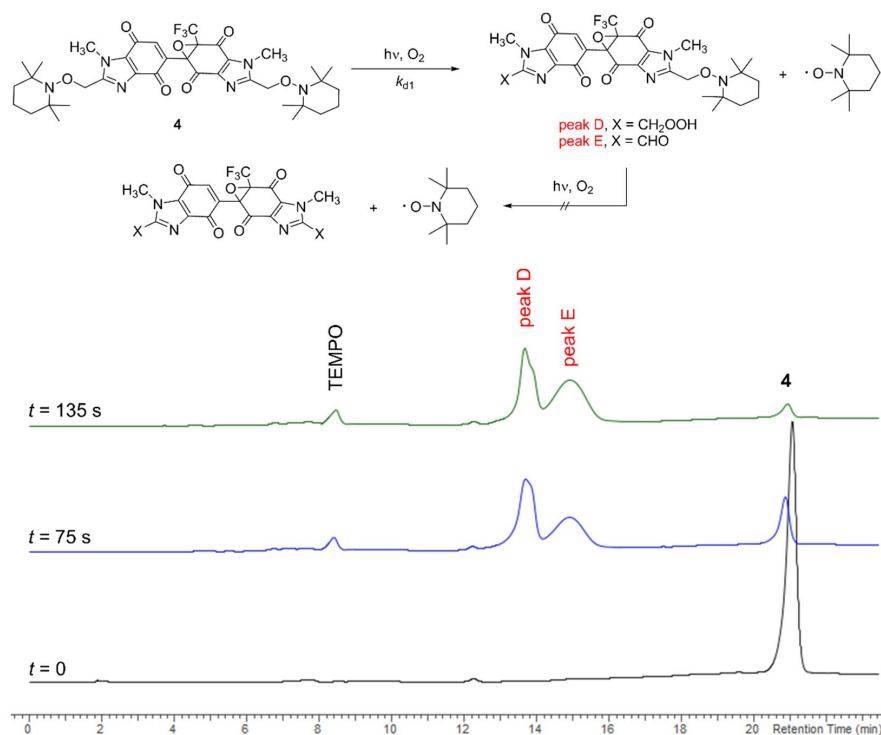


Figure S3 HPLC-MS (ESI) monitoring of the blue LED homolysis of (A) **Bis-TEMPO-Vis** and (B) epoxide-quinone **4**. The [M + H]⁺ adducts were detected and used to assign the structures corresponding to peaks A, B, D and E. The [M + Na + MeCN]⁺ adduct was used to assign the major component of a complex mixture in peak C. The accuracy of all HRMS data was better than 5 ppm compared to the predicted masses.

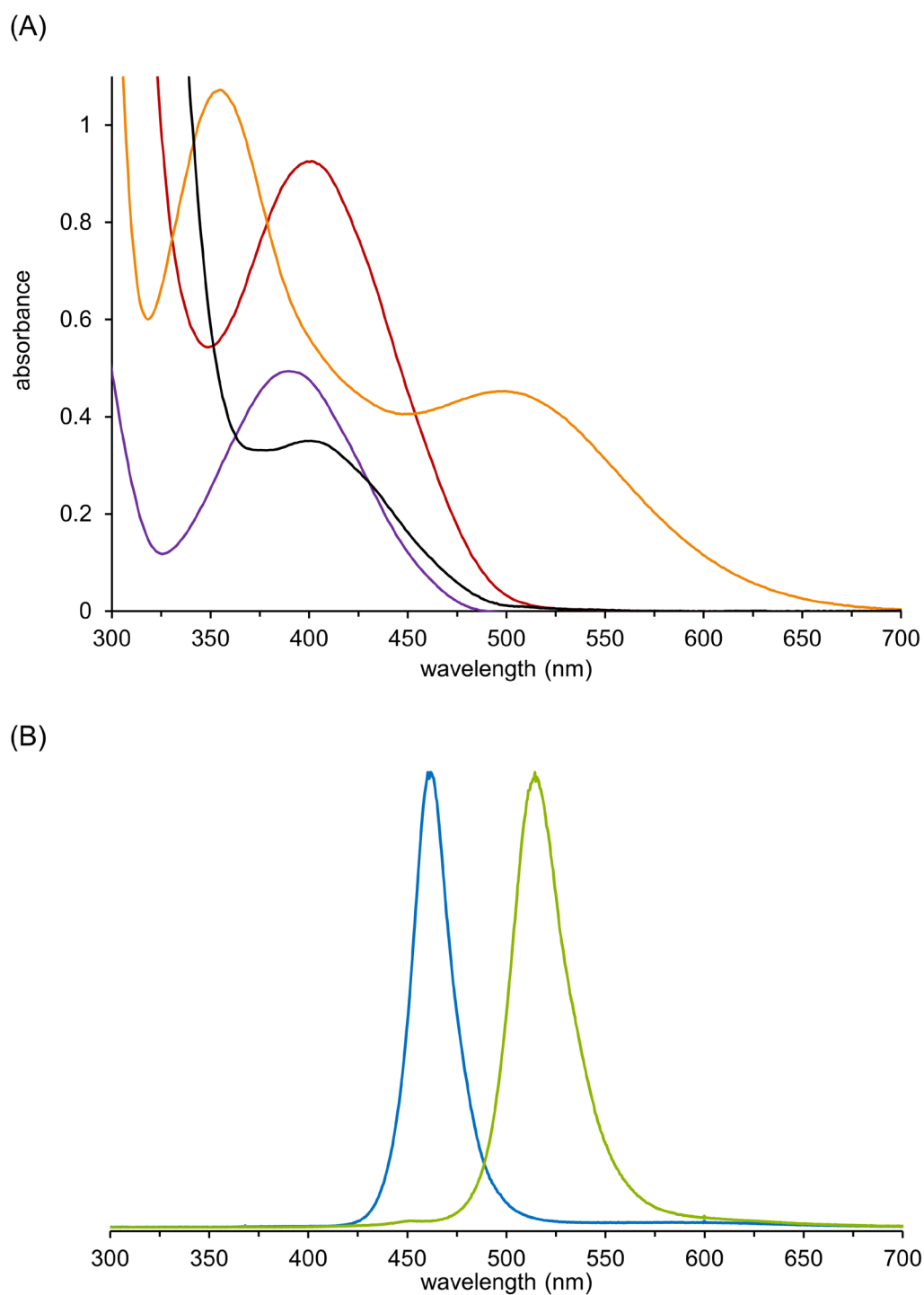


Figure S4 (A) UV-visible light absorption spectra recorded in DCE (all 3.75×10^{-4} M) of **TEMPO-Vis** (purple), dimethoxybenzimidazole-benzimidazolequinone **2** (orange), **Bis-TEMPO-Vis** (red) and epoxide-quinone **4** (black). (B) Emission spectra for blue and green LEDs.

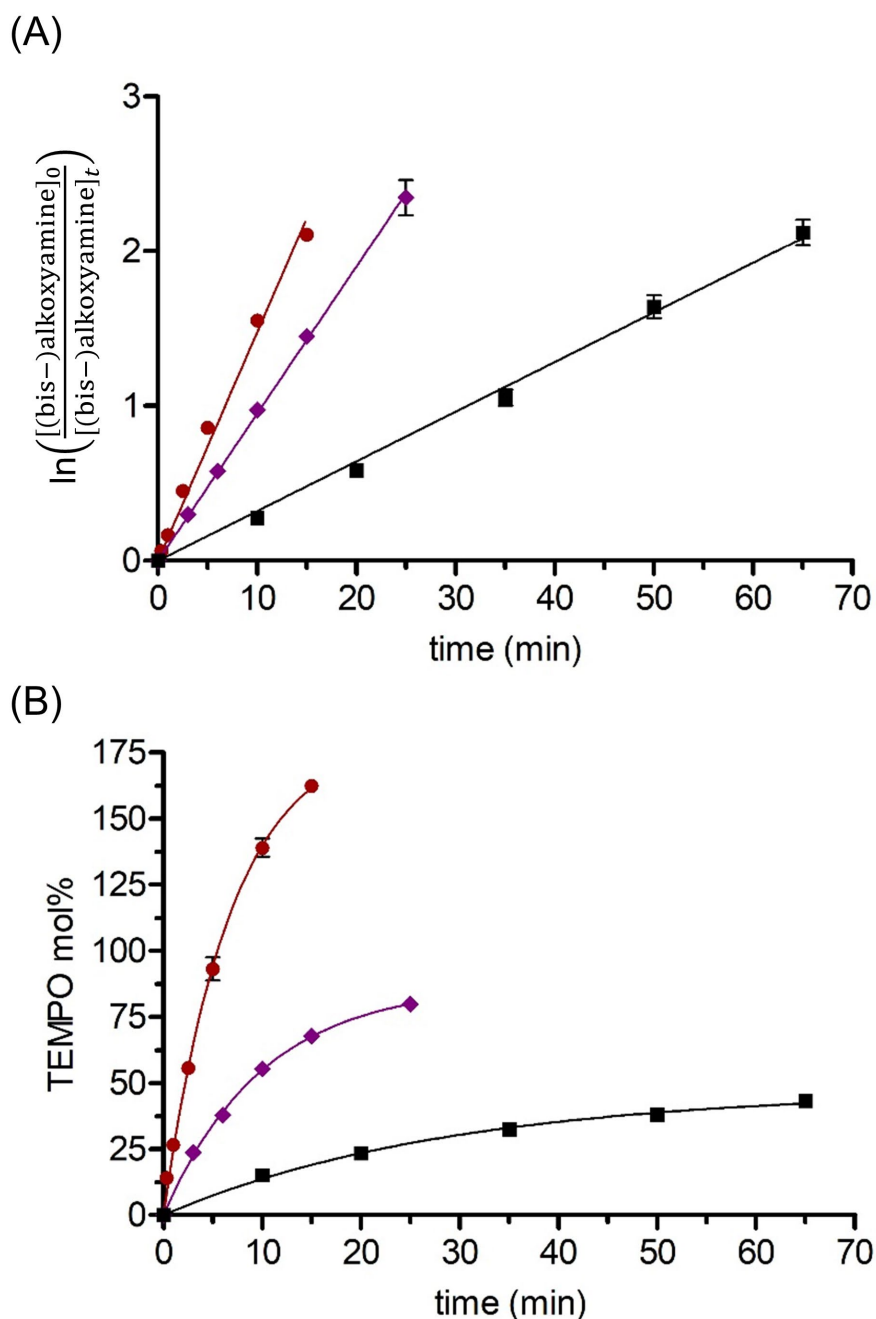
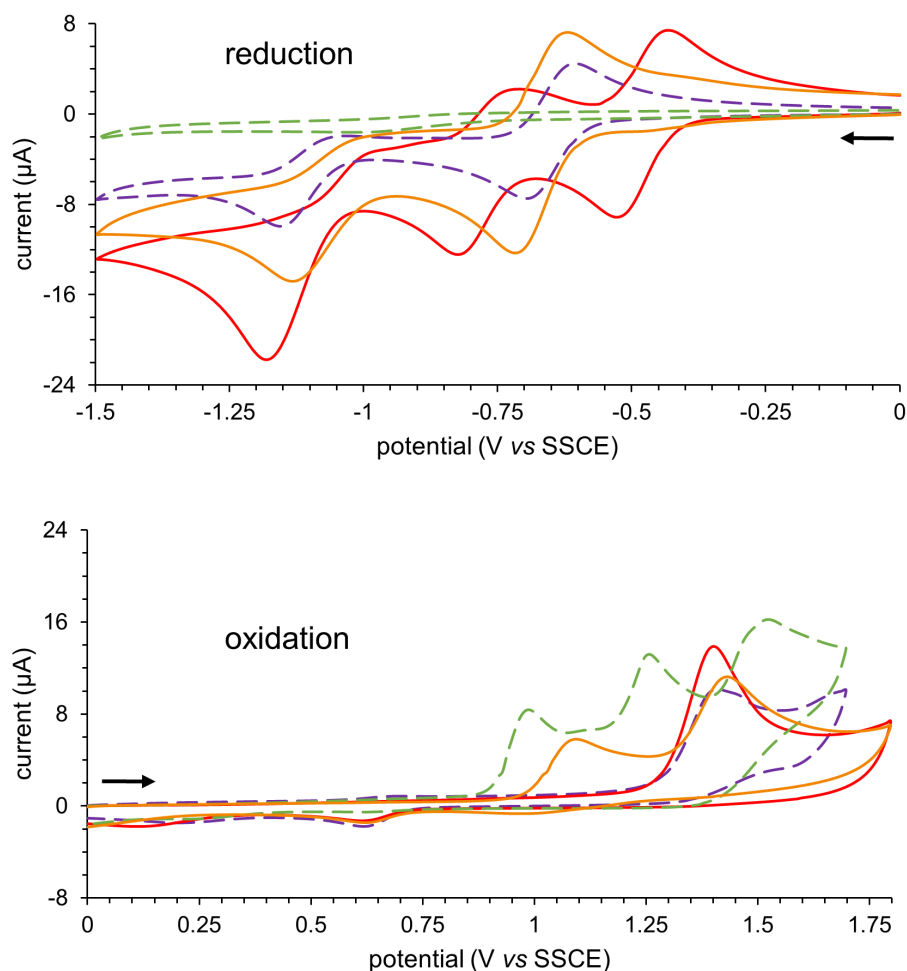


Figure S5 Kinetics (at rt) of alkoxyamine and bis-alkoxyamine homolysis in green LED according to (A) (bis-)alkoxyamine decay and (B) TEMPO release. Eq 1 was fitted to the plots in (B) using GraphPad Prism software. Key: **TEMPO-Vis** (—◆—), **Bis-TEMPO-Vis** (—●—) and **4** (—■—). Conditions: alkoxyamine (0.25 mM, DCE) illuminated by two green LED bulbs (9 W each) under O₂ balloon, with HPLC analysis. Experiments performed in triplicate.

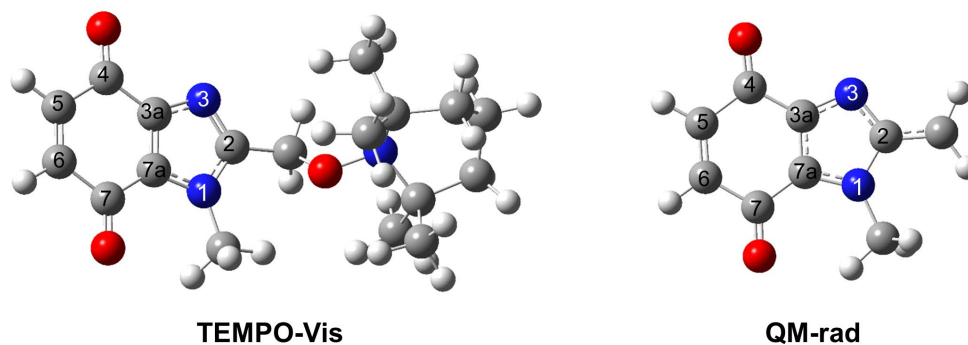


	reduction			oxidation	
	$Q_1/Q_1^{\cdot-}$	$Q_2/Q_2^{\cdot-}$	$Q^{\cdot-}/Q^{2-}$	DMB/DMB ^{ox}	Q/Q^{ox}
2	-0.67	-	-1.13 (irrev)	1.09 (irrev)	1.43 (irrev)
TEMPO-Vis	-0.65	-	-1.16 (irrev)	-	1.41 (irrev)
1	-	-	-	0.99 (irrev)	-
Bis-TEMPO-Vis	-0.48	-0.77	-1.18 (irrev)	-	1.40 (irrev)

Figure S6 Cyclic voltammetry of **Bis-TEMPO-Vis** (—), **TEMPO-Vis** (---), **2** (—) and **1** (---) with associated table of redox potentials (all in V). The first reduction of **2** correlates with the first quinone reduction ($Q_1/Q_1^{\cdot-}$) of **TEMPO-Vis**, indicating that the LUMO of **2** lies on the quinone motif. The first oxidation of **2** correlates well with the first oxidation of dimethoxybenzimidazole (DMB/DMB^{ox}) **1**, indicating that the HOMO of **2** lies on the dimethoxybenzimidazole motif. For **Bis-TEMPO-Vis**, the two quinone moieties are electronically coupled resulting in two consecutive *one-electron* reductions ($Q_1/Q_1^{\cdot-} = -0.48$ V and $Q_2/Q_2^{\cdot-} = -0.77$ V), and a further *two-electron* reduction at -1.18 V correlated to the second ($Q^{\cdot-}/Q^{2-}$) one-electron reduction of **TEMPO-Vis**. The first oxidation of **Bis-TEMPO-Vis** correlates with the equivalent process in **TEMPO-Vis**. Scan rate of 0.1 V/s, alkoxyamine (1 mM), anhydrous DCE (with Bu₄NPF₆ as electrolyte, 0.2 M), arrow indicates direction of scan.

Supporting Tables

Table S1 DFT-derived bond lengths in the benzimidazolequinone core of **TEMPO-Vis** and **QM-rad**^a



bond	TEMPO-Vis length (Å)	QM-rad length (Å)
1N—CH ₃	1.459	1.456
1N—2C	1.366	1.388
1N—7aC	1.366	1.361
2C—CH ₂	1.493	1.389
2C—3N	1.319	1.354
3N—3aC	1.359	1.333
3aC—4C	1.475	1.483
3aC—7aC	1.377	1.395
4C—O	1.206	1.205
4C—5C	1.504	1.499
5C—6C	1.336	1.336
6C—7C	1.495	1.496
7C—O	1.213	1.216
7C—7aC	1.462	1.458

^aDFT geometry optimization performed in the gas phase using M06-2X (for **TEMPO-Vis**) or UM06-2X (for **QM-rad**) and 6-311++G (d,p), specifying singlet multiplicity for **TEMPO-Vis** and doublet multiplicity for **QM-rad**.

Table S2 Quantum yields of homolysis (Φ_h)^a

	LED color	Φ_h (%) ^b
TEMPO-Vis	blue	6.19
Bis-TEMPO-Vis	blue	2.56
4	blue	1.17
2	blue	0.003
TEMPO-Vis	green	0.047
Bis-TEMPO-Vis	green	0.074
4	green	0.016
2	green	< 0.0001

^aHomolysis performed according to Table 2 conditions using blue LED (1 × 9 W) or green LED (2 × 9 W) bulbs. ^bCalculated from the number of alkoxyamine molecules consumed during the half-life ($t_{1/2}$) of decay and the total number of available photons (see equation S1 below). Low Φ_h are reported in other visible-light photolysis.^{2,3}

Experimental

Materials

2-(Chloromethyl)-4,7-dimethoxy-1-methyl-1*H*-benzimidazole was prepared from (4,7-dimethoxy-1*H*-benzimidazol-2-yl)methanol^{4,5} using NaH (Sigma-Aldrich, 60% dispersion in mineral oil) and MeI (Sigma-Aldrich, > 99%) in THF for *N*-methylation, followed by treatment with SOCl₂ (Sigma-Aldrich, 97%) in CH₂Cl₂ (Fischer Scientific, ≥ 99%) for chlorination. (2,2,6,6-Tetramethylpiperidin-1-yl)oxyl (TEMPO, Sigma-Aldrich, 98%), H₂ (BOC, 99.99%), PtO₂ (Sigma-Aldrich), MgSO₄ (Alfa Aesar, 99.5%), Na₂CO₃ (ACROS Organics, 99.5%), *N*-bromosuccinimide (NBS, Lancaster, 99%), H₂SO₄ (BDH, 98%), [bis(trifluoroacetoxy)iodo]benzene (PIFA, Sigma-Aldrich, 97%), MeCN (Sigma-Aldrich, HPLC Plus, ≥ 99.9%), cerium(IV) ammonium nitrate (CAN, Fischer Scientific, 99%), *t*BuOOH (ACROS Organics, 70% in H₂O), sodium trifluoromethanesulfinate (Langlois reagent, TCI, > 95%), Ar (BOC, 99.8%), Cu(OTf)₂ (Sigma-Aldrich, 98%), 1,2-dichloroethane (DCE, Sigma-Aldrich, anhydrous, 99.8%), Bu₄NPF₆ (Sigma-Aldrich, for electrochemical analysis, ≥ 99%), EtOAc (Fischer Scientific, ≥ 99%) and hexanes (Fischer Scientific, bp 40–60 °C) were used as received. THF (Sigma-Aldrich, CHROMASOLV® Plus ≥ 99.9%) and Et₂O (Sigma-Aldrich, > 99.5%) were dried and distilled over Na (Sigma-Aldrich, > 99.8%) and benzophenone (ACROS Organics, 99%). CDCl₃ (Sigma-Aldrich, 99.8% atom D + 0.03% Si(CH₃)₄ v/v) and CD₂Cl₂ (Eurisotop, 99.9% atom D) were used as received. Thin layer chromatography (TLC) was performed on Merck TLC silica gel 60 F₂₅₄ plates using a UV lamp (254 nm) for visualization. Flash chromatography was performed using silica gel, pore size 60 Å, 230–400 mesh, and particle size 40–63 µm. Dry column vacuum chromatography (with Apollo Scientific silica gel ZEOprep 60 and 15–35 µm particle size),⁶ was preferable for purification of light-active compounds, due to the convenience of light exclusion by covering the apparatus with Al-foil during elution.

Measurements

DFT calculations: Geometry optimizations were performed using Gaussian 16,⁷ installed at the Irish Centre for High-End Computing (ICHEC), using an M06-2X functional⁸ with a 6-311++G (d,p) basis set. All structures were fully optimized in the gas phase and verified as local minima through frequency calculations. The unrestricted formalism, UM06-2X, was specified for all radical models. The natural bond orbital (NBO) energy calculation on **QM-**

rad was performed using M06-2X with a cc-pVTZ basis set. TD-DFT was performed at the same level of theory as the geometry optimization, with 1,2-dichloroethane (DCE) as solvent using the polarizable continuum model (PCM).⁹ Natural transition orbitals (NTOs) provided graphical representation of the ground and excited states.¹⁰ Bond dissociation energies (BDEs) were calculated based on the free energy difference between the starting alkoxyamines and the radical products (thermal free energy correction was added). The lowest triplet energies (E_T) of starting alkoxyamines are given relative to the optimized singlet ground state (S_0) energies. Model energies are reported in Table A1 of the appendix.

Melting points, ultraviolet-visible and infrared spectroscopy: Melting points were measured on a Stuart Scientific melting point apparatus SMP3. Ultraviolet-visible (UV-vis) spectra were recorded using a Varian (Cary 100) UV-vis spectrometer. Infrared spectra were recorded using a Perkin-Elmer Spec 1 with ATR attached.

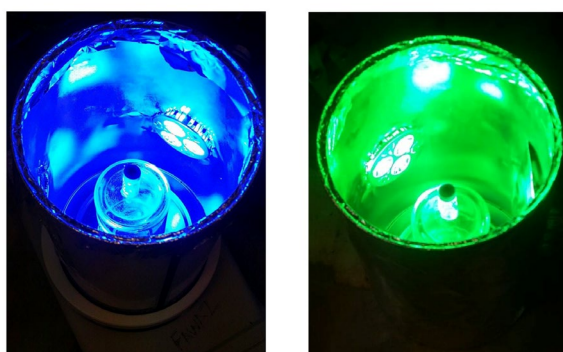
Nuclear magnetic resonance (NMR spectroscopy): NMR spectra were recorded using a JEOL ECX 400 MHz or a Varian 500 or 600 MHz instrument (the specific NMR frequency used is detailed in the characterization section and on spectra). The chemical shifts were in ppm relative to $\text{Si}(\text{CH}_3)_4$ for recorded spectra in CDCl_3 , and relative to CH_2Cl_2 at 5.32 ppm for ^1H NMR and 53.84 ppm for ^{13}C NMR spectra recorded in CD_2Cl_2 . ^{13}C NMR data were collected at 100, 125 or 150 MHz with complete proton decoupling. NMR assignments were supported by DEPT and ^1H - ^1H (COSY) and ^1H - ^{13}C single bond correlation (HSQC). Multiple bond correlation of ^1H - ^{13}C (HMBC) was used to characterize the aromatic CHs in benzimidazolequinone-dimethoxybenzimidazoles **2** and **3**, with through-space correlation (ROESY) supplementing the CH characterization in trifluoromethylquinone **3**. ^{19}F NMR data were collected at 470 MHz.

High resolution mass spectrometry (HRMS): HRMS was carried out using ESI time-of-flight mass spectrometer (TOFMS) in positive mode using a Waters LCT Mass Spectrometry instrument. The precision of all accurate mass measurements was better than 5 ppm.

Single crystal X-ray diffraction: Single crystal data was collected using an Oxford Diffraction Xcalibur system operated using the CrysAlisPro software. The crystal structure was solved using ShelxT version 2014/55,¹¹ and refined using ShelxL version 2017/1,¹² both of which were operated within the Oscale software package.¹³ Crystallographic data for **Bis-TEMPO-Vis** has been deposited with the Cambridge Crystallographic Data Centre with deposit number CCDC-1948448. This data is available free of charge via

www.ccdc.cam.ac.uk/data_request/cif (or from the Cambridge Crystallographic Data Centre, 12 Union Road, Cambridge CB2 1EZ, U.K.; fax +44 1223 336033; or e-mail deposit@ccdc.cam.ac.uk). Single crystal X-ray data and structure refinements are reported in Table A2 of the appendix.

Visible-light photoreactor: The reactor used blue (1×9 W) or green (2×9 W) LED bulb(s) placed inside an aluminium container of diameter 10 cm (below). A vial (1.5 mL capacity for homolysis kinetics experiments, Table 2) with a solution of alkoxyamine was placed in the centre of the reactor opposite the bulb. The bulb was air cooled using a 2.5 W fan, which ensured that the interior reactor temperature remained at ambient temperature. The emission spectra of the LEDs were narrow and confined to the visible region (Figure S4B).



Analytical HPLC: The Agilent 1100 Series HPLC was equipped with a UV detector operating at 254 nm and a Phenomenex® BondClone™ 10 μ m C18, 250 \times 4.6 mm column. The sample was injected via automatic injector (see table below for injection volume). The flow rate of the mobile phase was 1 mL/min, and the composition depended on the experiment being performed (see below). Calibration curves were generated for [TEMPO] and [alkoxyamine] for the construction of rate plots, and for the determination of k_d .

homolysis experiment	injection volume (μ L)	mobile phase program (%MeCN in H ₂ O)
TEMPO-Vis	5	time 0 = 45, 11.5 min = 45, 15 min = 75, 19.5 min = 75, 19.6 min = 45, 22 min = 45
Bis-TEMPO-Vis and 4	10	time 0 = 45, 15 min = 95, 19 min = 95, 19.5 min = 45, 23 min = 45
2	5	time 0 = 45, 11.5 min = 45, 15 min = 95, 27 min = 95, 27.1 min = 45, 30 min = 45

Homolysis rates (k_d): A solution of alkoxyamine in DCE (1 mL, 0.25 mM) in a 1.5 mL clear glass vial was prepared in the absence of light. A sample was taken and analyzed by HPLC (representing time 0). The solution was subjected to either one blue (9 W) LED bulb or two green (9 W) LED bulbs under an O₂ balloon for a period of time. A sample was taken and [TEMPO] and [alkoxyamine] were measured by HPLC. During the run, the remainder of the solution was placed in the dark, which stopped the reaction, as evidenced by the on/off experiment (Figure S2). Illumination of the solution was resumed, with continued sampling over time. Experiments were performed in triplicate. Rate constants (k_d) were derived using two equivalent methods: (1) using the first-order plot describing the decay of [alkoxyamine] over time and (2) using the growth of [TEMPO] and fitting eq 1 using the method of least squares within GraphPad Prism® software.

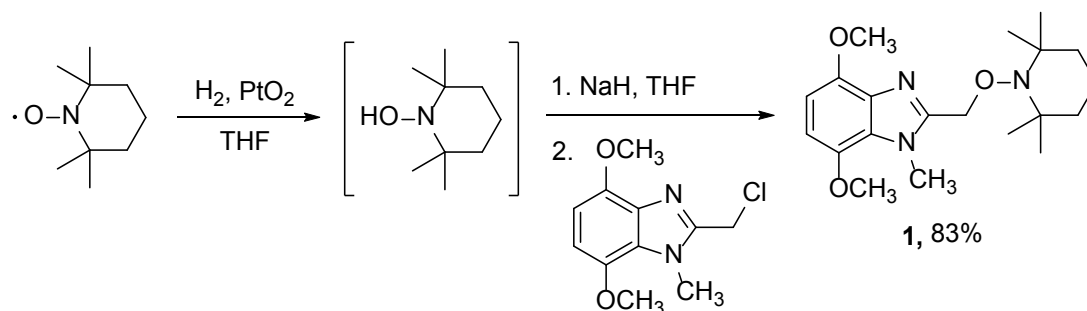
Quantum yield of homolysis (Φ_h): The Φ_h was measured according to eq S1. The number of molecules converted was calculated based on the $t_{1/2}$ of the alkoxyamine starting material measured by alkoxyamine decay (Table 2). The number of incident photons was measured using a Wavetek DM15XL multimeter connected to a calibrated Thorlabs FDS1010 Si photodiode (1 cm²), and was calculated based on the total light intensity falling on the surface of the reaction vessel from two directions: one direction measuring light emanating directly from the bulb, and the other direction being 180° opposite, accounting for any reflection from the photoreactor interior.

$$\Phi_h = 100 \times \frac{\text{number of molecules converted}}{\text{number of incident photons}} \quad (\text{S1})$$

Cyclic voltammetry: Cyclic voltammograms were recorded using a PalmSens3+ potentiostat equipped with a glassy carbon and Pt-wire electrode, using a sodium-saturated calomel electrode (SSCE) as reference. Cycles were performed on alkoxyamines (1 mM) at a scan rate of 0.1 V/s in anhydrous DCE using Bu₄NPF₆ (0.2 M) as supporting electrolyte.

Synthetic Procedures and Characterization

Synthesis of 4,7-dimethoxy-1-methyl-2-[(2,2,6,6-tetramethylpiperidin-1-yl)oxy]methyl}-1*H*-benzimidazole (**1**)



TEMPO (0.972 g, 6.23 mmol) and PtO_2 (28 mg, 0.12 mmol) in THF (15 mL) were stirred under a balloon of H_2 at rt, until the mixture turned colourless (~ 2 h).¹⁴ The mixture was filtered, NaH (83 mg, 2.08 mmol, 60%) added, and stirred at rt for 1 h. 2-(Chloromethyl)-4,7-dimethoxy-1-methyl-1*H*-benzimidazole (0.50 g, 2.08 mmol) was added, and the stirring continued at reflux for 16 h. H_2O (50 mL) was added, and the solution extracted using CH_2Cl_2 (3×40 mL). The combined organic layers were dried (MgSO_4), evaporated, and the residue purified by flash chromatography using EtOAc and hexanes as eluent to give **1** (0.625 g, 83%) as a white solid; mp 114–116 °C; R_f 0.40 (2 : 3 EtOAc : hexanes); ν_{max} (neat, cm^{-1}) 2976, 2928, 1524, 1461, 1394, 1334, 1262, 1234, 1146, 1100, 1069, 1027; δ_{H} (400 MHz, CDCl_3) 1.05 (6H, s), 1.25 (6H, s), 1.29–1.31 (1H, m), 1.44–1.50 (5H, m), 3.85 (3H, s), 3.92 (3H, s), 4.11 (3H, s, NCH_3), 5.02 (2H, s), 6.45 (1H, d, $J = 8.5$ Hz), 6.52 (1H, d, $J = 8.5$ Hz); δ_{C} (100 MHz, CDCl_3) 17.1 (CH_2), 20.1 (CH_3), 33.1 (NCH_3), 33.5 (CH_3), 39.8 (CH_2), 55.8, 56.0 (both OCH_3), 60.1 (C), 72.0 (CH_2), 101.0, 103.3 (both CH), 126.9, 134.4, 141.8, 146.2, 149.8 (all C); HRMS (ESI) m/z $[\text{M} + \text{H}]^+$, $\text{C}_{20}\text{H}_{32}\text{N}_3\text{O}_3$ calcd. 362.2444, observed 362.2444.

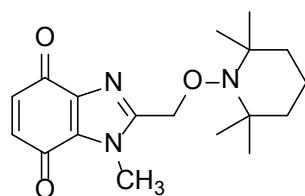
General procedures (A-C) for the synthesis of benzimidazolequinones via dimethoxybenzimidazole oxidations

Procedure A: *N*-Bromosuccinimide (NBS, 39 mg, 0.22 mmol) was added to dimethoxybenzimidazole **1** (72 mg, 0.20 mmol), H_2SO_4 (18 μL , 0.34 mmol) and THF/ H_2O (6 mL, 2/1) at rt, and stirred for 10 min in the absence of light. Aq Na_2CO_3 (10 mL, sat.) was added, and the solution was extracted with CH_2Cl_2 (2×20 mL). The combined organic layers

were dried (MgSO₄), evaporated, and the residue purified by dry column vacuum chromatography with EtOAc and hexanes as eluent.

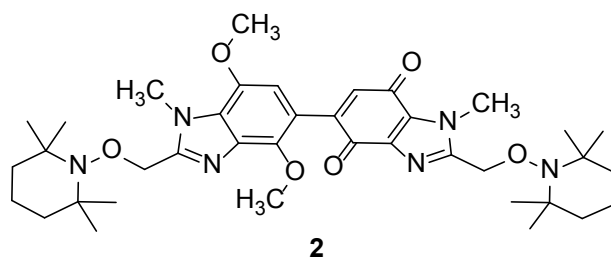
Procedure B: Bis[(trifluoroacetoxy)iodo]benzene (PIFA, 0.129 g, 0.30 mmol) in MeCN/H₂O (2 mL, 2/1) was added dropwise to dimethoxybenzimidazole **1** (72 mg, 0.20 mmol) in MeCN/H₂O (2 mL, 2/1) at rt, and stirred for 3 h in the absence of light. H₂O (10 mL) was added, and the solution extracted with CH₂Cl₂ (3 × 15 mL). The combined organic layers were dried (MgSO₄), evaporated, and the residue purified by dry column vacuum chromatography with EtOAc and hexanes as eluent.

Procedure C: Cerium(IV) ammonium nitrate (CAN, X mmol, see Table 1) in H₂O (5 mL) was added dropwise to dimethoxybenzimidazole **1** (72 mg, 0.20 mmol) in MeCN (5 mL) at 0 °C, and stirred for 20 min in the absence of light. H₂O (10 mL) was added, and the solution extracted with CH₂Cl₂ (3 × 15 mL). The combined organic layers were dried (MgSO₄), evaporated, and the residue purified by dry column vacuum chromatography with EtOAc (or Et₂O) and hexanes as eluent.

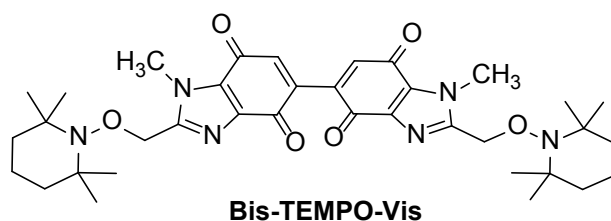


TEMPO-Vis

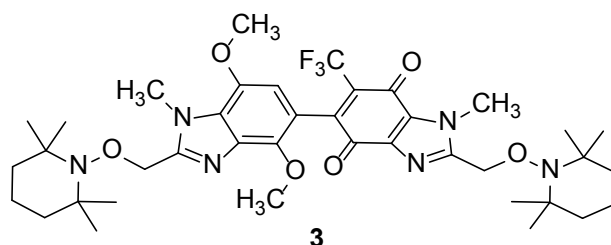
1-Methyl-2-([(2,2,6,6-tetramethylpiperidin-1-yl)oxy]methyl)-1H-benzimidazole-4,7-dione (TEMPO-Vis), according to Procedure B: 52 mg, 78%; yellow solid; mp 131–132 °C; *R*_f 0.50 (2: 3 EtOAc : hexanes); λ_{max} (DCE, nm) 389 ($\epsilon = 1.32 \times 10^3$); ν_{max} (neat, cm⁻¹) 2974, 2931, 1661 (C=O), 1591, 1515, 1478, 1375, 1361, 1347, 1336, 1276, 1202, 1132; δ_{H} (500 MHz, CDCl₃) 1.09 (6H, s, CH₃), 1.25 (6H, s, CH₃), 1.34–1.36 (2H, m), 1.48–1.51 (4H, m), 4.09 (3H, s), 5.02 (2H, s), 6.62 (1H, d, *J* = 10.5 Hz), 6.69 (1H, d, *J* = 10.5 Hz); δ_{C} (100 MHz, CDCl₃) 17.0 (CH₂), 20.2, 32.9, 33.3 (all CH₃), 39.8 (CH₂), 60.3 (C), 70.9 (CH₂), 131.5 (C), 136.3, 136.6 (both CH), 141.0, 151.4 (both C), 178.8, 181.1 (both C=O); HRMS (ESI) *m/z* [M + H]⁺, C₁₈H₂₆N₃O₃ calcd. 332.1974, observed 332.1971.



4',7'-Dimethoxy-1,1'-dimethyl-2,2'-bis{[(2,2,6,6-tetramethylpiperidin-1-yl)oxy]methyl}-1H,1'H-[5,5'-bibenzimidazole]-4,7-dione (2), according to Procedure C using CAN (0.219 g, 0.40 mmol): 0.119 g, 86%; deep red solid; mp 127–129 °C; R_f 0.25 (1 : 1 EtOAc : hexanes); λ_{\max} (DCE, nm) 497 ($\epsilon = 1.20 \times 10^3$), 355 ($\epsilon = 2.87 \times 10^3$); ν_{\max} (neat, cm^{-1}) 2972, 2930, 1653 (C=O), 1532, 1463, 1277, 1150, 1103, 1037; δ_{H} (400 MHz, CDCl_3) 1.05–1.06 (12H, m, CH_3), 1.23 (12H, s, CH_3), 1.29–1.32 (2H, m), 1.45–1.50 (10H, m), 3.86 (3H, s, OCH_3), 4.08 (3H, s, NCH_3), 4.09 (3H, s, NCH_3), 4.15 (3H, s, OCH_3), 5.00 (2H, s), 5.01 (2H, s), 6.43 (1H, s, C6'-H), 6.66 (1H, s, C6-H); δ_{C} (100 MHz, CDCl_3) 17.0, 17.1 (both CH_2), 20.2 (CH_3), 32.9, 33.1 (both NCH_3), 33.3, 33.4 (both CH_3), 39.8 (CH_2), 56.0 (OCH_3), 60.1, 60.3 (C), 61.5 (OCH_3), 71.0, 72.0 (both CH_2), 105.4 (C6'-H), 116.8, 128.7, 131.5 (all C), 134.3 (C6-H), 136.4, 141.3, 142.7, 144.3, 147.0, 150.5, 151.1 (all C), 179.0, 180.1 (both C=O); HRMS (ESI) m/z $[\text{M} + \text{H}]^+$, $\text{C}_{38}\text{H}_{55}\text{N}_6\text{O}_6$ calcd. 691.4183, observed 691.4183.

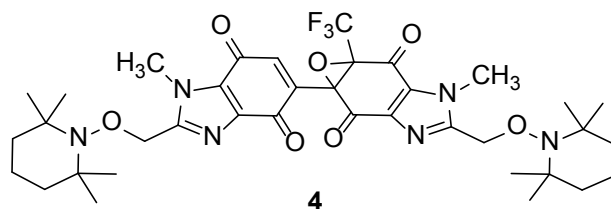


1,1'-Dimethyl-2,2'-bis{[(2,2,6,6-tetramethylpiperidin-1-yl)oxy]methyl}-1H,1'H-5,5'-bibenzimidazole-4,4',7,7'-tetrone (Bis-TEMPO-Vis), according to Procedure C using CAN (0.350 g, 0.64 mmol): 0.108 g, 82%; yellow solid; mp 228–231 °C (deg); R_f 0.28 (19 : 1 Et_2O : hexanes); λ_{\max} (DCE, nm) 401 ($\epsilon = 2.35 \times 10^3$), 273 ($\epsilon = 1.89 \times 10^4$); ν_{\max} (neat, cm^{-1}) 2975, 2934, 2870, 1662 (C=O), 1533, 1519, 1479, 1447, 1371, 1279, 1244, 1183, 1112, 1048; δ_{H} (500 MHz, CD_2Cl_2) 1.12 (12H, s), 1.27 (12H, s), 1.35–1.37 (4H, m), 1.46–1.57 (8H, bs), 4.08 (6H, s, NCH_3), 4.91–5.13 (4H, bs), 6.69 (2H, s); δ_{C} (150 MHz, CD_2Cl_2) 16.9 (CH_2), 19.8 (CH_3), 32.7 (NCH_3), 32.9 (CH_3), 39.6 (CH_2), 60.1 (C), 70.7 (CH_2), 131.7 (C), 136.0 (CH), 140.4, 140.7, 151.7 (all C), 177.4, 178.5 (both C=O); HRMS (ESI) m/z $[\text{M} + \text{H}]^+$, $\text{C}_{36}\text{H}_{49}\text{N}_6\text{O}_6$ calcd. 661.3714, observed 661.3716.



Synthesis of 4',7'-dimethoxy-1,1'-dimethyl-2,2'-bis{[(2,2,6,6-tetramethylpiperidin-1-yl)oxy]methyl}-6-(trifluoromethyl)-1H,1'H-[5,5'-bibenzimidazole]-4,7-dione (3**)**

*t*BuOOH (133 μ L, 70% in H_2O , 1.11 mmol) was added dropwise to 5,5'-dimethoxybenzimidazole-benzimidazolequinone **2** (0.18 g, 0.26 mmol), $NaSO_2CF_3$ (0.122 g, 0.78 mmol), and $Cu(OTf)_2$ (9 mg, 0.03 mmol) in MeCN (3 mL) at rt under Ar. After 2 h of stirring, H_2O (15 mL) was added, and the precipitate filtered. Purification of the precipitate by flash chromatography using EtOAc and hexanes as eluent gave trifluoromethylquinone **3** as a deep red oil (0.106 g, 54%); R_f 0.43 (2 : 3 EtOAc : hexanes); ν_{max} (neat, cm^{-1}) 2973, 2931, 1670 (C=O), 1611, 1502, 1466, 1375, 1361, 1297, 1262, 1245, 1175, 1130, 1041, 990; δ_H (500 MHz, $CDCl_3$) 1.09–1.11 (12H, m, CH_3), 1.24–1.38 (14H, m), 1.49–1.55 (10H, m), 3.85 (3H, s, OCH_3), 4.13 (3H, s, NCH_3), 4.15 (3H, s, NCH_3), 4.16 (3H, s, OCH_3), 5.038 (2H, s), 5.043 (2H, s), 6.27 (1H, s); δ_C (125 MHz, $CDCl_3$) 16.9, 17.0 (both CH_2), 20.1 (CH_3), 32.9, 33.1 (both NCH_3), 33.2 (CH_3), 39.66, 39.72 (both CH_2), 55.9 (OCH_3), 60.1, 60.2 (both C), 61.1 (OCH_3), 70.8, 71.7 (both CH_2), 104.5 (CH), 113.8 (C), 121.7 (q, $J = 276.6$ Hz, CF_3), 128.7 (C), 130.6 (q, $J = 27.5$ Hz, C6), 131.2, 135.4, 140.5, 142.1, 143.2, 147.84–147.85 (m), 150.2, 152.3 (all C), 174.6, 178.1 (both C=O); δ_F (470 MHz, $CDCl_3$) – 56.69; HRMS (ESI) m/z $[M + H]^+$, $C_{39}H_{54}N_6O_6F_3$ calcd. 759.4057, observed 759.4066.



3-Methyl-6a-(1-methyl-4,7-dioxo-2-{[(2,2,6,6-tetramethylpiperidin-1-yl)oxy]methyl}-4,7-dihydro-1H-benzimidazol-5-yl)-4-{[(2,2,6,6-tetramethylpiperidin-1-yl)oxy]methyl}-1a-(trifluoromethyl)-1aH-oxireno[f]benzimidazole-2,6(3H,6aH)-dione (4**)**, according to procedure A: 116 mg, 78%; yellow solid; mp 150–152 $^{\circ}C$ (deg); R_f 0.56 (3 : 7 EtOAc : hexanes); λ_{max} (DCE, nm) 400 ($\epsilon = 9.31 \times 10^2$), 313 ($\epsilon = 5.60 \times 10^3$); ν_{max} (neat, cm^{-1}) 2931,

1695 (C=O), 1664 (C=O), 1517, 1477, 1361, 1292, 1212, 1182, 1126, 1034; δ_{H} (500 MHz, CDCl_3) 1.10 (12H, s), 1.21–1.25 (12H, m), 1.33–1.36 (2H, m), 1.43–1.56 (10H, bs), 4.11 (3H, s, NCH_3), 4.13 (3H, s, NCH_3), 5.02 (2H, s), 5.03 (2H, s), 6.78 (1H, s); δ_{C} (125 MHz, CDCl_3) 16.90, 16.93 (both CH_2), 20.08, 20.11 (both CH_3), 32.9, 33.19, 33.25, 33.4 (all CH_3), 39.67, 39.69 (both CH_2), 60.2, 60.3 (both C), 63.4 (q, $J = 33.9$ Hz, C- CF_3), 65.6 (C), 70.72, 70.74 (both CH_2), 120.4 (q, $J = 280.7$ Hz, CF_3), 131.3, 132.2 (both C), 135.1 (CH), 138.9, 140.2, 140.4, 151.8, 154.2 (all C), 176.1, 176.9, 178.1, 179.5 (all C=O); δ_{F} (470 MHz, CDCl_3) – 65.81; HRMS (ESI) m/z $[\text{M} + \text{H}]^+$, $\text{C}_{37}\text{H}_{48}\text{N}_6\text{O}_7\text{F}_3$ calcd. 745.3537, observed 745.3547.

References in Supplementary Information

1. D. J. Van Hoomissen and S. Vyas, *J. Org. Chem.*, 2017, **82**, 5731. <https://doi.org/10.1021/acs.joc.7b00549>.
2. A. Paul, A. Biswas, S. Sinha, S. S. Shah, M. Bera, M. Mandal and N. D. P. Singh, *Org. Lett.*, 2019, **21**, 2968. <https://doi.org/10.1021/acs.orglett.9b00124>.
3. Y. Chen and M. G. Steinmetz, *Org. Lett.*, 2005, **17**, 3729. <https://doi.org/10.1021/ol051362k>.
4. M. A. Phillips, *J. Chem. Soc.*, 1928, 2393. <https://doi.org/10.1039/JR9280002393>.
5. A. Gellis, H. Kovacic, N. Boufatah and P. Vanelle, *Eur. J. Med. Chem.*, 2008, **43**, 1858. <https://doi.org/10.1016/j.ejmech.2007.11.020>.
6. L. M. Harwood, *Aldrichimica Acta*, 1985, **18**, 25.
7. M. J. Frisch, G. W. Trucks, H. B. Schlegel, G. E. Scuseria, M. A. Robb, J. R. Cheeseman, G. Scalmani, V. Barone, G. A. Petersson, H. Nakatsuji, X. Li, M. Caricato, A. V. Marenich, J. Bloino, B. G. Janesko, R. Gomperts, B. Mennucci, H. P. Hratchian, J. V. Ortiz, A. F. Izmaylov, J. L. Sonnenberg, D. Williams-Young, F. Ding, F. Lipparini, F. Egidi, J. Goings, B. Peng, A. Petrone, T. Henderson, D. Ranasinghe, V. G. Zakrzewski, J. Gao, N. Rega, G. Zheng, W. Liang, M. Hada, M. Ehara, K. Toyota, R. Fukuda, J. Hasegawa, M. Ishida, T. Nakajima, Y. Honda, O. Kitao, H. Nakai, T. Vreven, K. Throssell, J. A. Montgomery, Jr., J. E. Peralta, F. Ogliaro, M. J. Bearpark, J. J. Heyd, E. N. Brothers, K. N. Kudin, V. N. Staroverov, T. A. Keith, R. Kobayashi, J. Normand, K. Raghavachari, A. P. Rendell, J. C. Burant, S. S. Iyengar, J. Tomasi, M. Cossi, J. M. Millam, M. Klene, C. Adamo, R. Cammi, J. W. Ochterski, R. L. Martin, K. Morokuma, O. Farkas, J. B. Foresman and D. J. Fox, Gaussian 16, Revision B.01, Gaussian, Inc., Wallingford CT, 2016.
8. Y. Zhao and D. G. Truhlar, *Theor. Chem. Acc.*, 2008, **120**, 215. <https://doi.org/10.1007/s00214-007-0310-x>.
9. C. Amovilli, V. Barone, R. Cammi, E. Cancès, M. Cossi, B. Mennucci, C. S. Pomelli and J. Tomasi, *J. Adv. Quant. Chem.*, 1998, **32**, 227. [https://doi.org/10.1016/S0065-3276\(08\)60416-5](https://doi.org/10.1016/S0065-3276(08)60416-5).
10. R. L. Martin, *J. Chem. Phys.*, 2003, **118**, 4775. <https://doi.org/10.1063/1.1558471>.
11. G. Sheldrick, *Acta Crystallogr. Sect. A: Found. Crystallogr.*, 2015, **71**, 3. <https://doi.org/10.1107/S2053273314026370>.
12. G. Sheldrick, *Acta Crystallogr. Sect. C: Cryst. Struct. Commun.*, 2015, **71**, 3. <https://doi.org/10.1107/S2053229614024218>.
13. P. McArdle, *J. Appl. Crystallogr.*, 2017, **50**, 320. <https://doi.org/10.1107/S1600576716018446>.
14. F. Aldabbagh, W. K. Busfield, I. D. Jenkins and S. H. Thang, *Tetrahedron Lett.*, 2000, **41**, 3673. [https://doi.org/10.1016/S0040-4039\(00\)00440-8](https://doi.org/10.1016/S0040-4039(00)00440-8).

Appendix

Tables Referenced in Supplementary Information

Table A1 DFT model energies associated with Table 2.

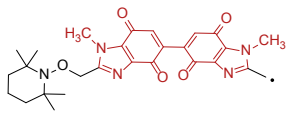
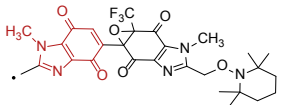
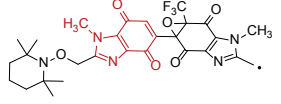
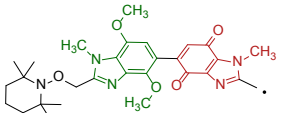
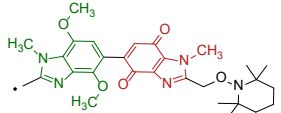
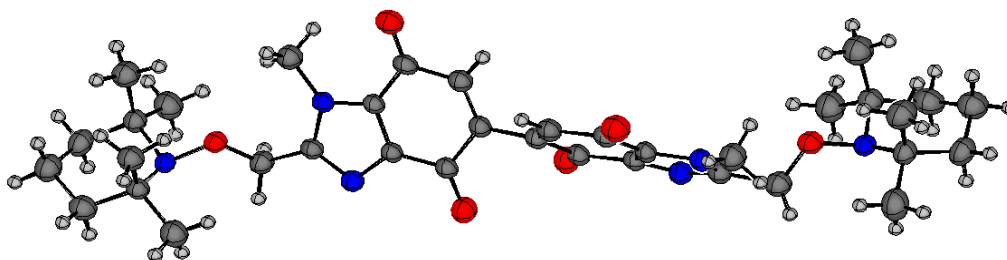
compd	multiplicity	EE (Hartrees)	EE + thermal free energy correction (Hartrees)
TEMPO-Vis	singlet	− 1090.676089	− 1090.311417
TEMPO-Vis	triplet	− 1090.594405	− 1090.232441
QM-rad	doublet	− 606.984531	− 606.875713
Bis-TEMPO-Vis	singlet	− 2180.186815	− 2179.453072
Bis-TEMPO-Vis	triplet	− 2180.103807	− 2179.371002
 Bis-TEMPO-Vis radical	doublet	− 1696.486519	− 1696.009845
4	singlet	− 2592.424110	− 2591.685608
4	triplet	− 2592.339550	− 2591.605755
 4 quinone-radical	doublet	− 2108.723751	− 2108.244338
 4 epoxide-radical	doublet	− 2108.723151	− 2108.242497
2	singlet	− 2259.989495	− 2259.180506
2	triplet	− 2259.921214	− 2259.113174
 2 quinone-radical	doublet	− 1776.289571	− 1775.737561
 2 dimethoxy-radical	doublet	− 1776.289116	− 1775.734596
TEMPO	doublet	− 483.631085	− 483.403280

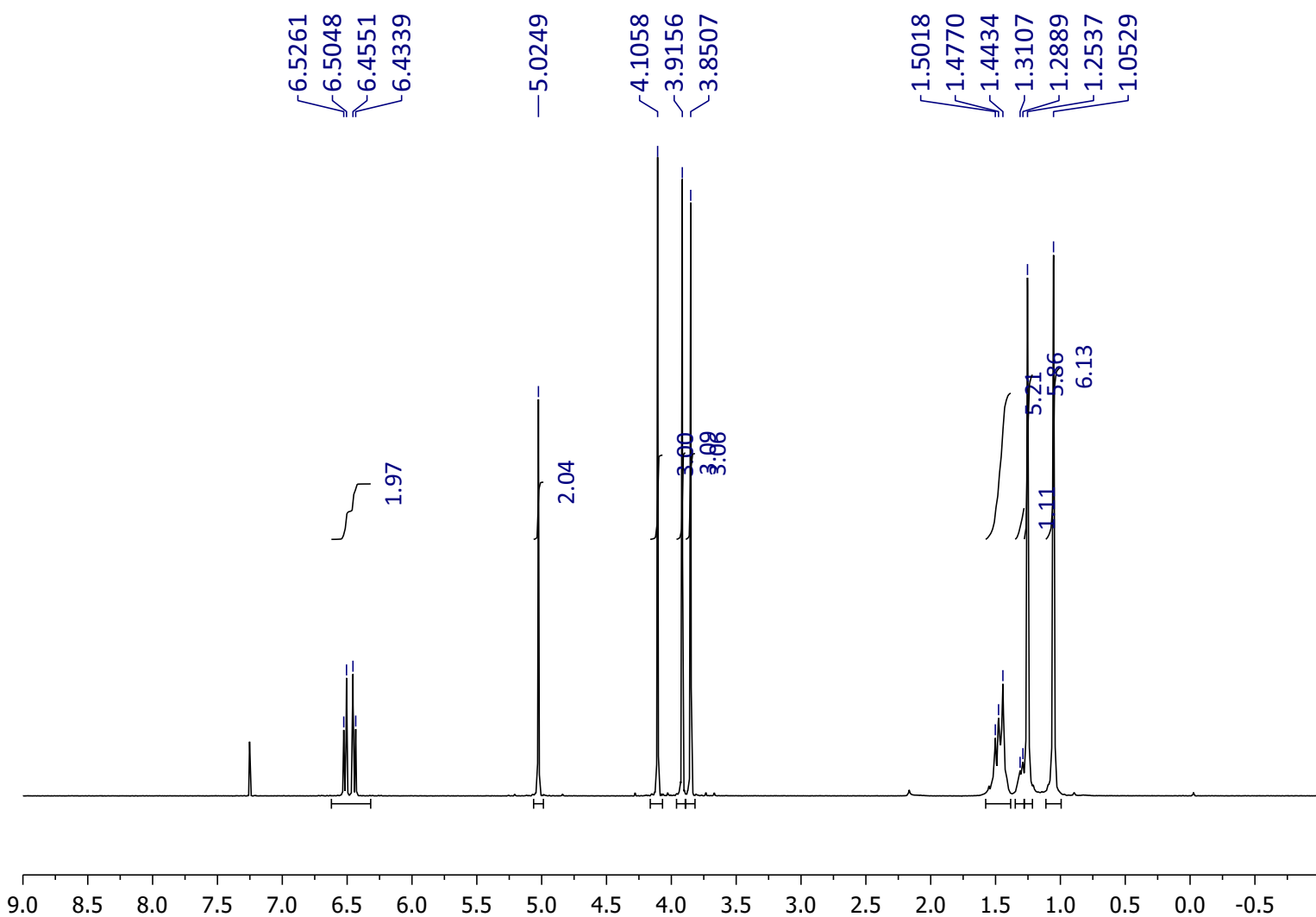
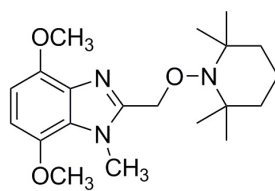
Table A2 Single crystal X-ray data and structure refinement for **Bis-TEMPO-Vis** (thermal ellipsoids set at 50% probability). The dihedral angle defined by C6-C5-C5'-C6' is 55.6°.



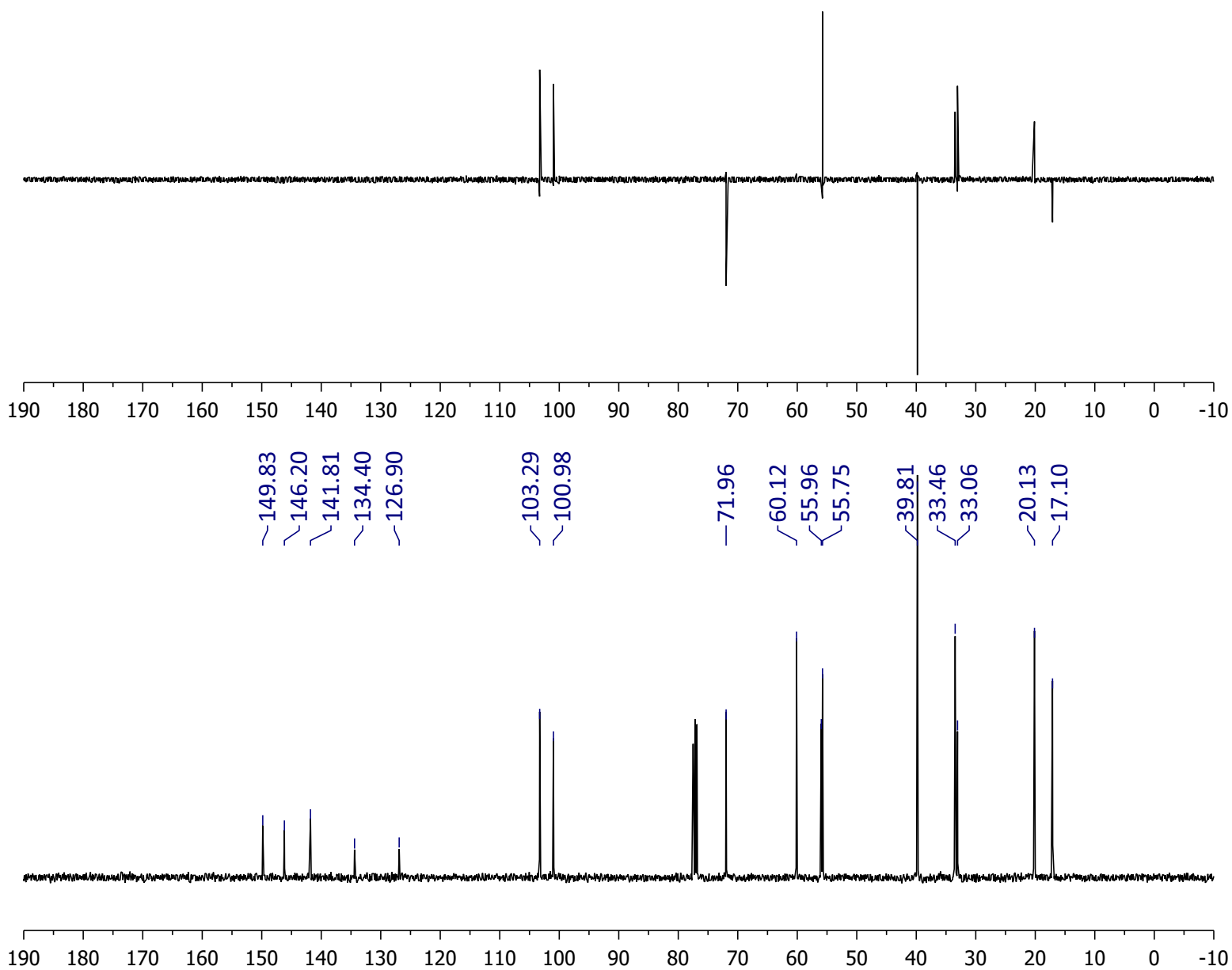
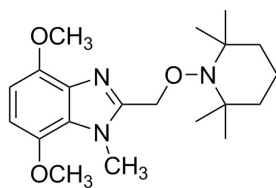
Empirical formula	C ₃₆ H ₄₈ N ₆ O ₆	
Formula weight	660.80	
Temperature	298.9(5) K	
Wavelength	0.71073 Å	
Crystal system	Orthorhombic	
Space group	P2 ₁ 2 ₁ 2 ₁	
Unit cell dimensions	a = 6.0407(3) Å	α = 90°.
	b = 21.1209(12) Å	β = 90°.
	c = 27.1076(14) Å	γ = 90°.
Volume	3458.5(3) Å ³	
Z	4	
Density (calculated)	1.269 Mg/m ³	
Absorption coefficient	0.087 mm ⁻¹	
F(000)	1416	
Crystal size	0.50 x 0.40 x 0.20 mm ³	
Theta range for data collection	3.455 to 29.311°.	
Index ranges	-6 ≤ h ≤ 8, -28 ≤ k ≤ 21, -32 ≤ l ≤ 35	
Reflections collected	28054	
Independent reflections	8461 [R(int) = 0.0449]	
Completeness to theta = 25.242°	99.6 %	
Absorption correction	Semi-empirical from equivalents	
Max. and min. transmission	1.00000 and 0.62048	
Refinement method	Full-matrix least-squares on F ²	
Data / restraints / parameters	8461 / 0 / 443	
Goodness-of-fit on F ²	1.002	
Final R indices [I > 2σ(I)]	R1 = 0.0519, wR2 = 0.1002	
R indices (all data)	R1 = 0.0942, wR2 = 0.1188	
Absolute structure parameter	0.7(5)	
Extinction coefficient	n/a	
Largest diff. peak and hole	0.167 and -0.196 e.Å ⁻³	

NMR Spectra

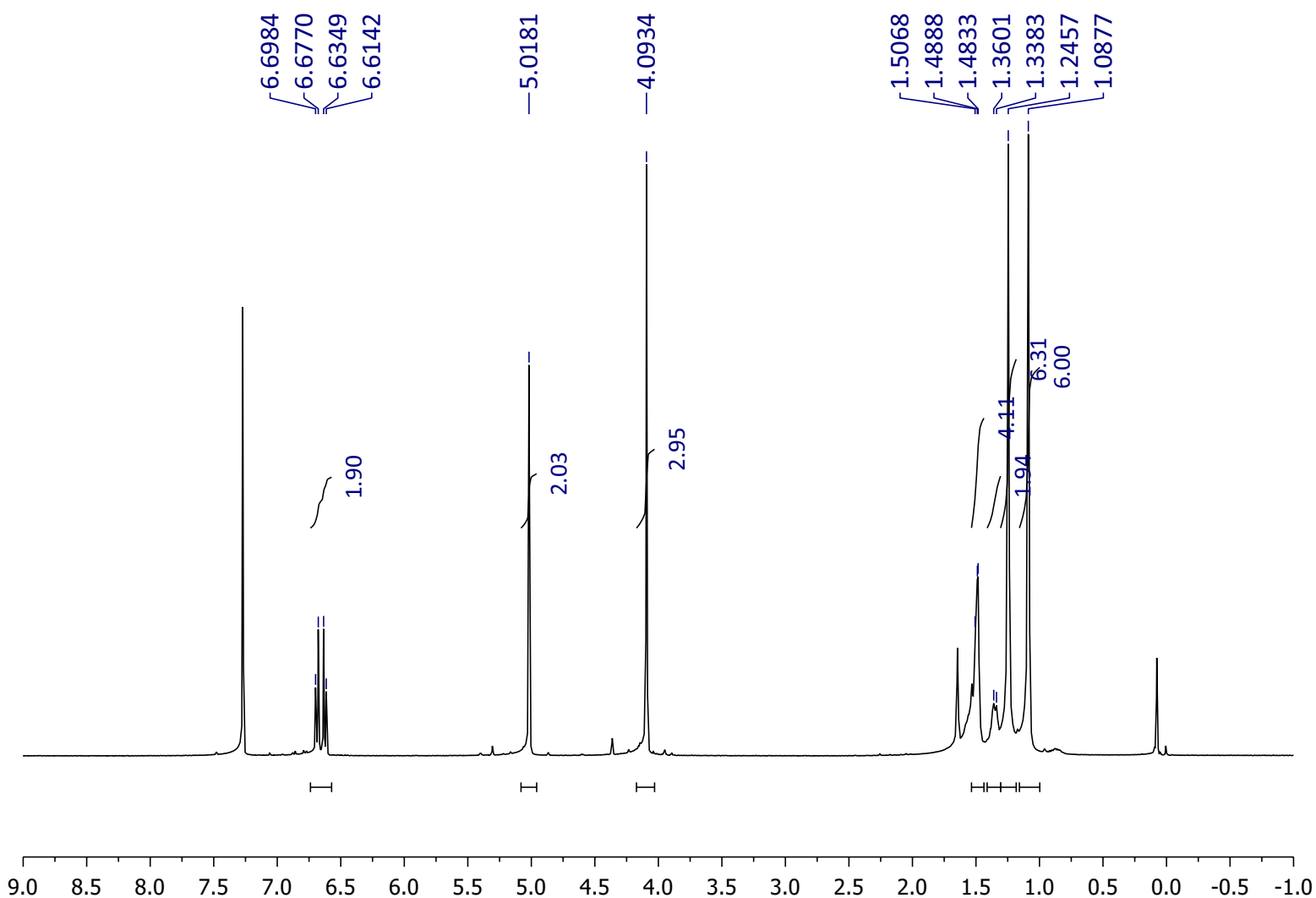
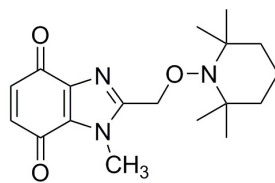
^1H NMR (400 MHz) of **1** in CDCl_3



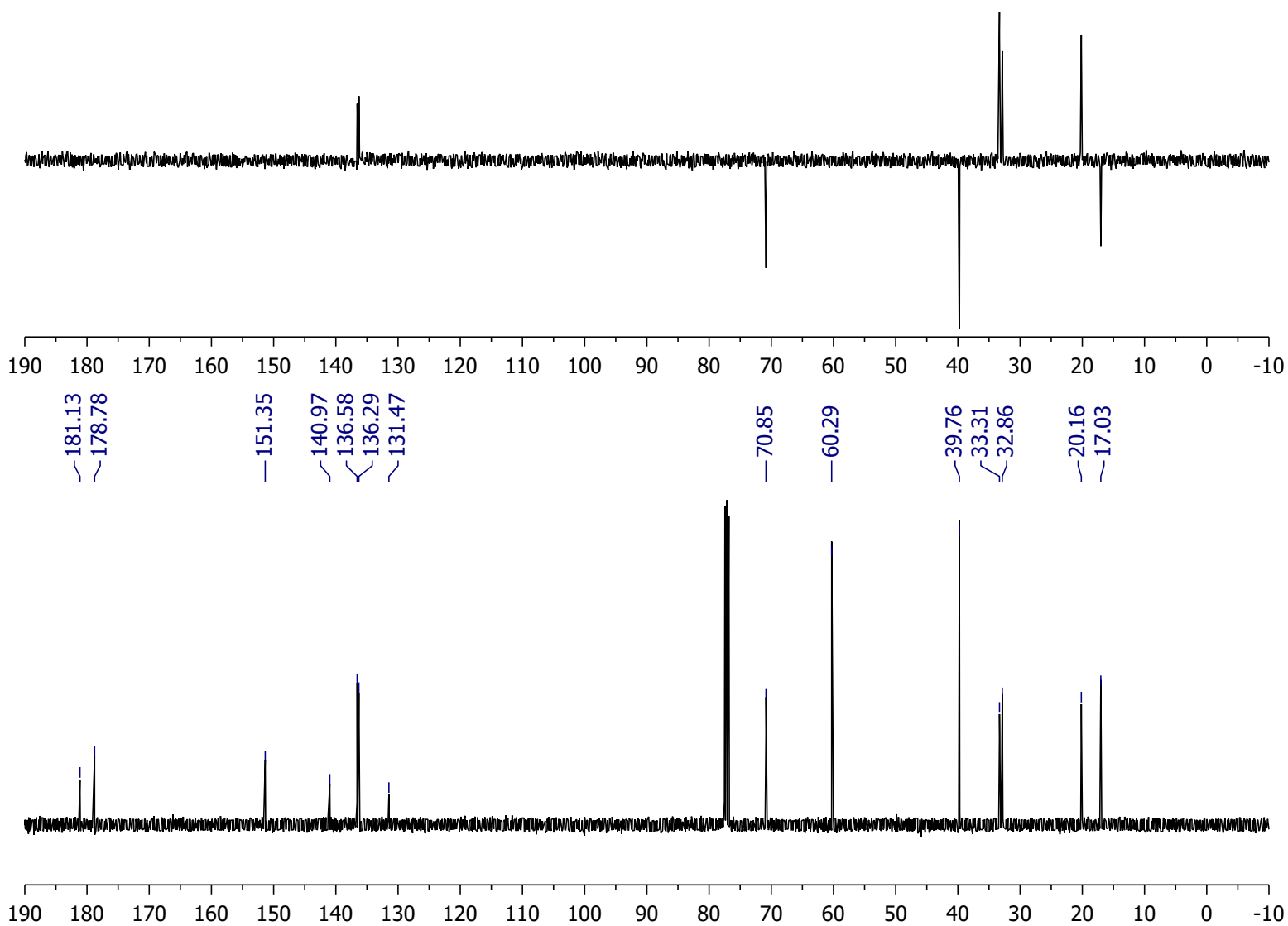
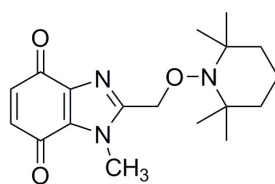
^{13}C NMR (100 MHz) of **1** in CDCl_3



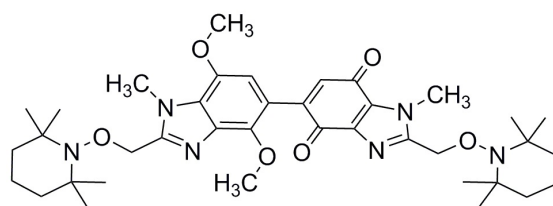
^1H NMR (500 MHz) of **TEMPO-Vis** in CDCl_3



^{13}C NMR (100 MHz) of **TEMPO-Vis** in CDCl_3



^1H NMR (400 MHz) of **2** in CDCl_3

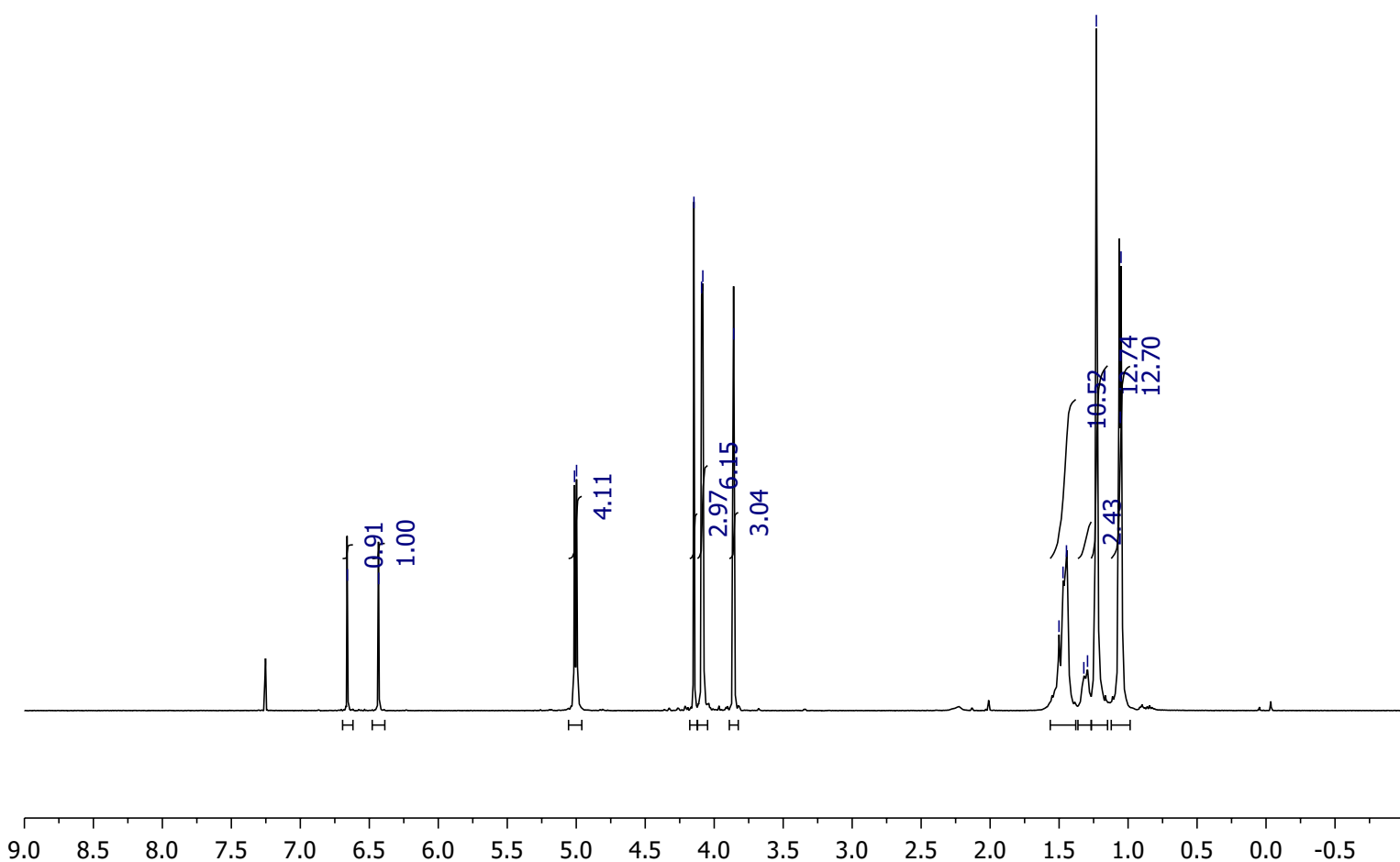


— 6.6589
— 6.4323

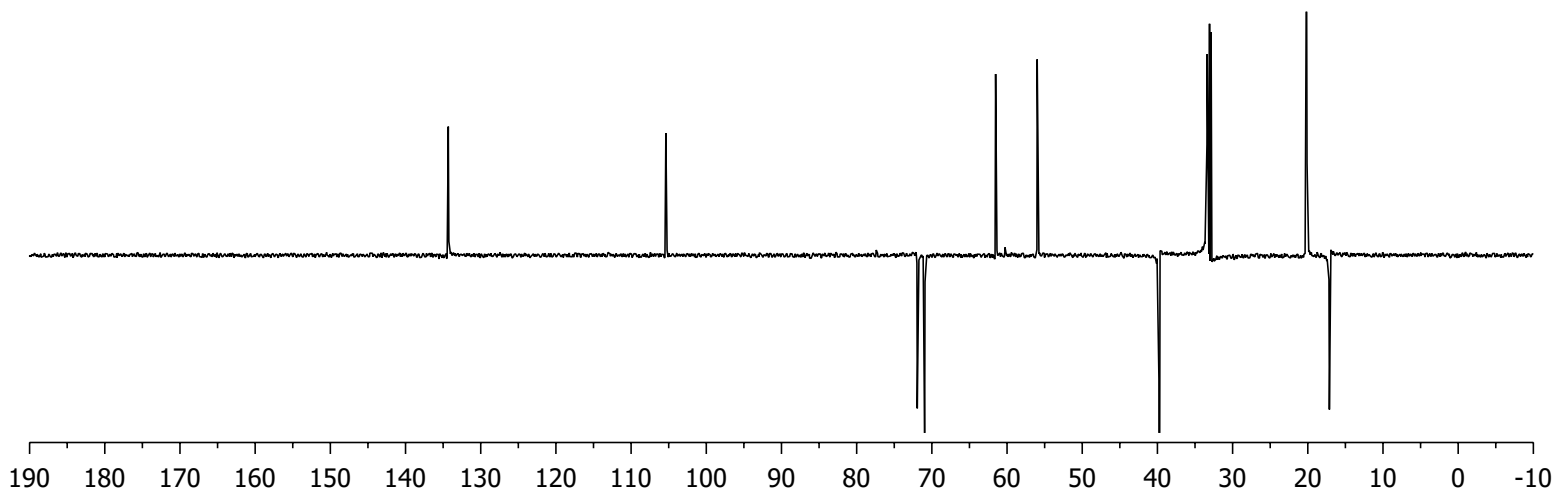
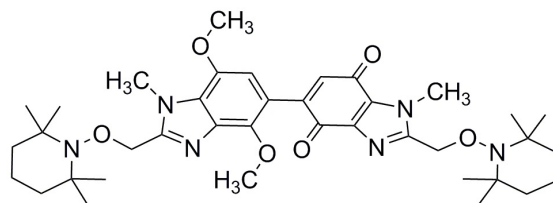
5.0126
4.9977

4.1470
4.0914
4.0824
3.8583

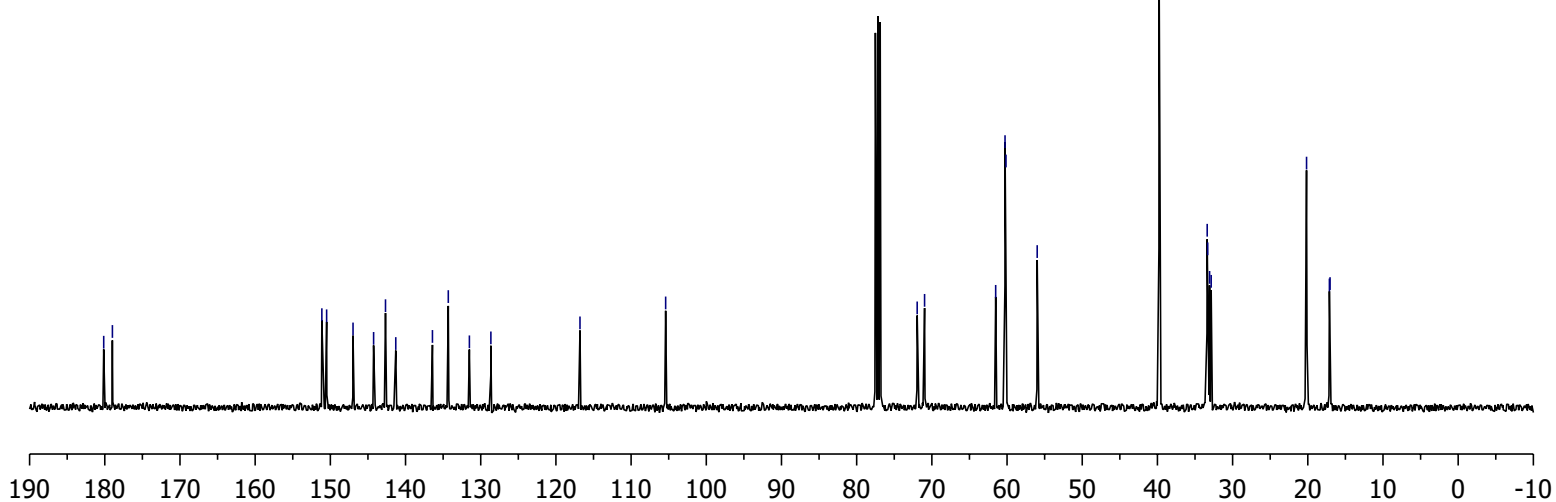
1.5008
1.4717
1.4467
1.3208
1.2939
1.2300
1.0565
1.0510



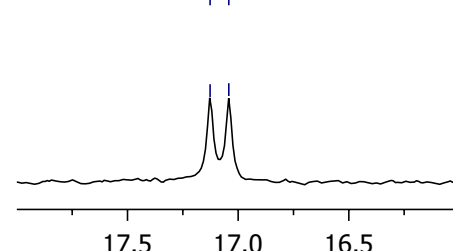
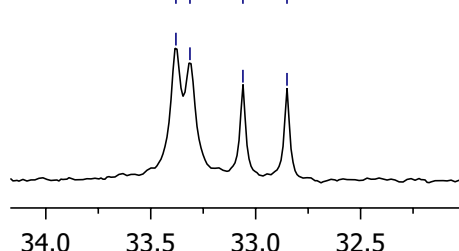
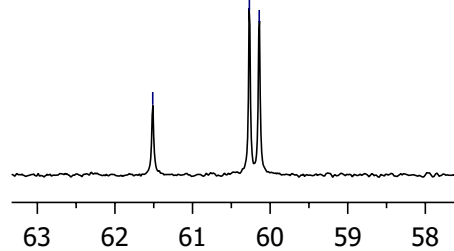
^{13}C NMR (100 MHz) of **2** in CDCl_3



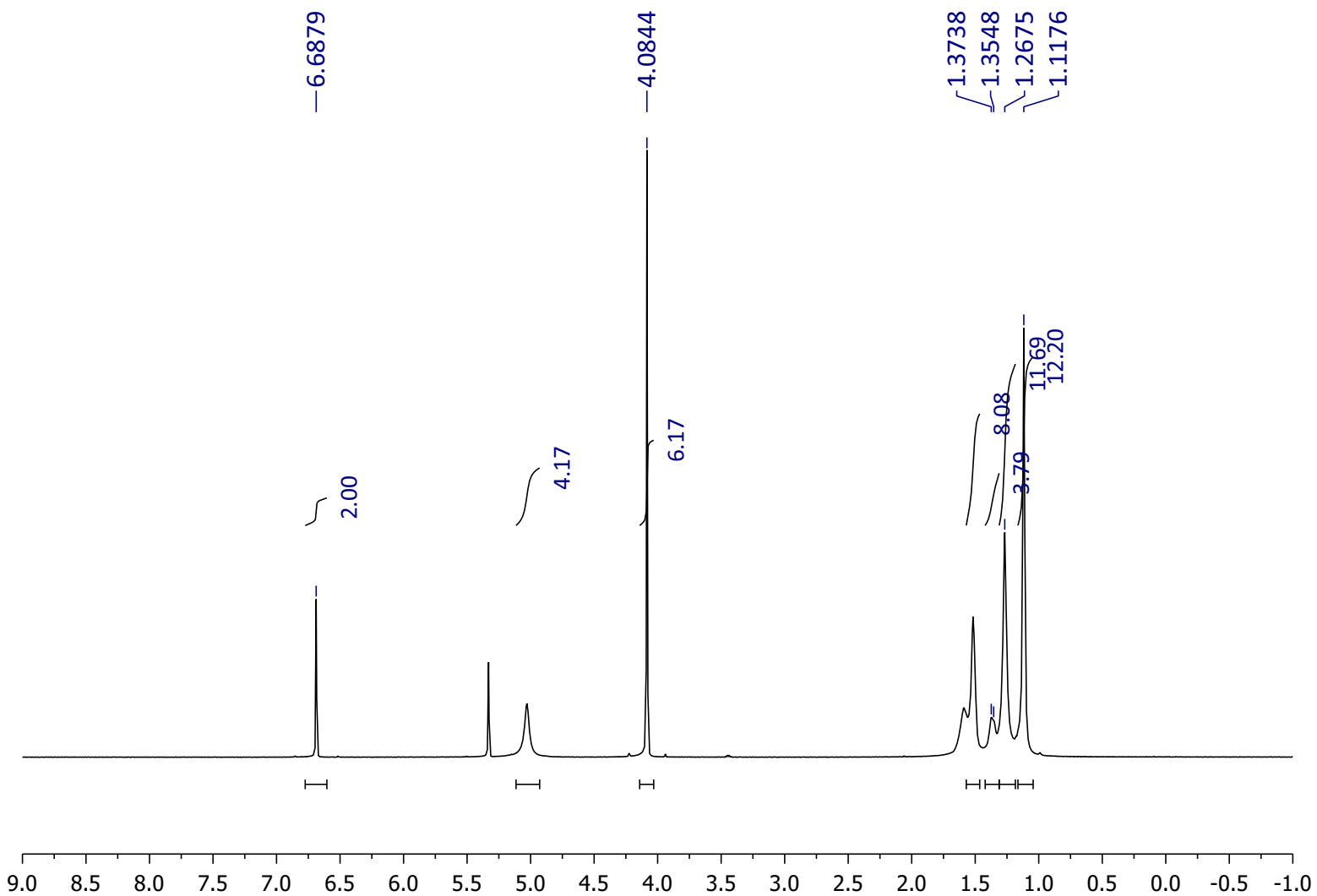
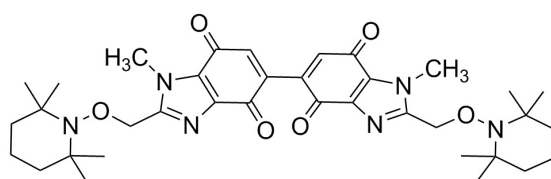
180.14, 178.99, 151.13, 150.50, 146.98, 144.25, 142.66, 141.30, 136.42, 134.31, 131.51, 128.65, 116.80, 105.40, 71.95, 70.97, 61.51, 60.27, 60.14, 55.99, 39.78, 33.38, 33.31, 33.06, 32.85, 20.17, 17.13, 17.04



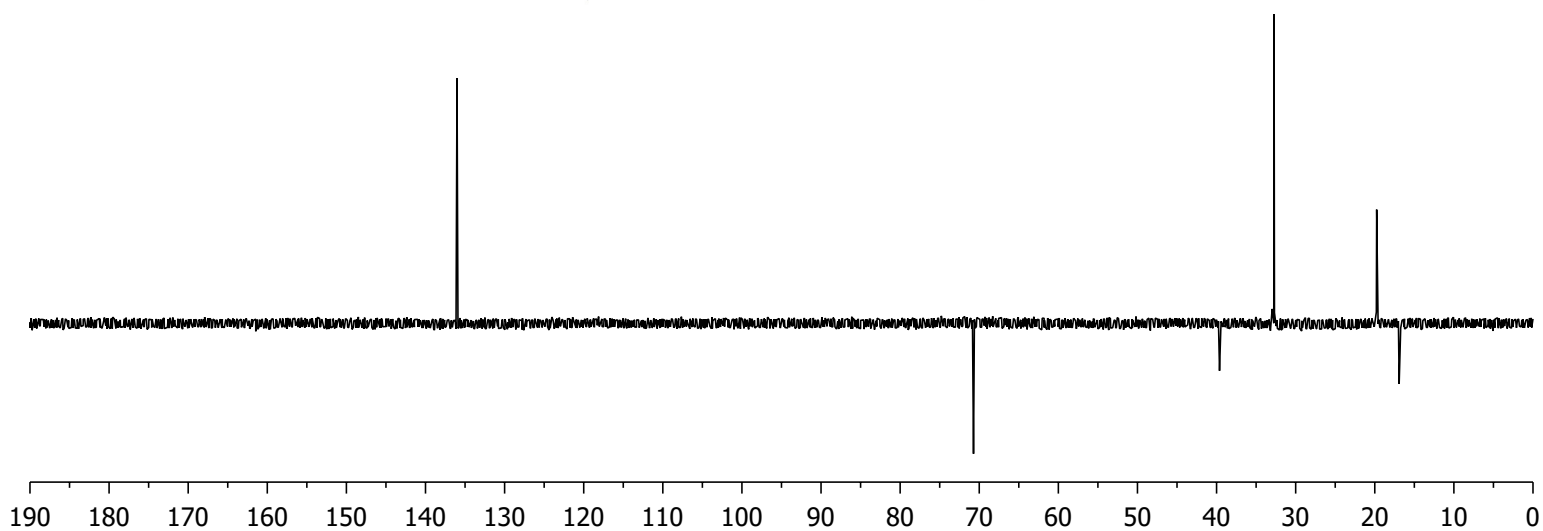
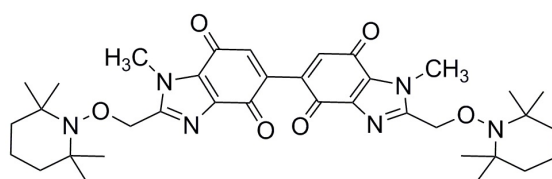
61.51, 60.27, 60.14, 33.38, 33.31, 33.06, 32.85, 17.13, 17.04



^1H NMR (500 MHz) of **Bis-TEMPO-Vis** in CD_2Cl_2



^{13}C NMR (150 MHz) of **Bis-TEMPO-Vis** in CD_2Cl_2



178.52
177.41

151.73

140.73

140.41

136.01

131.70

70.72

60.12

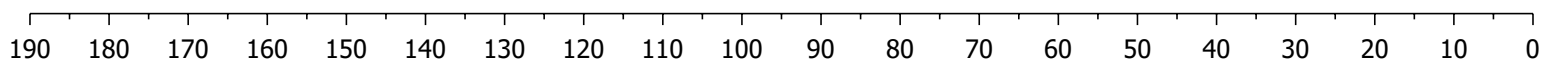
39.63

32.92

32.73

19.76

16.92



140.73

140.41

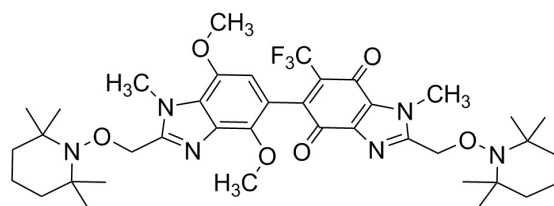
32.92

32.73

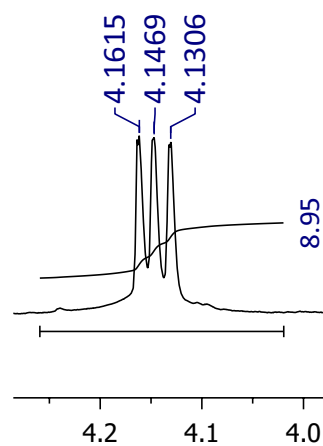
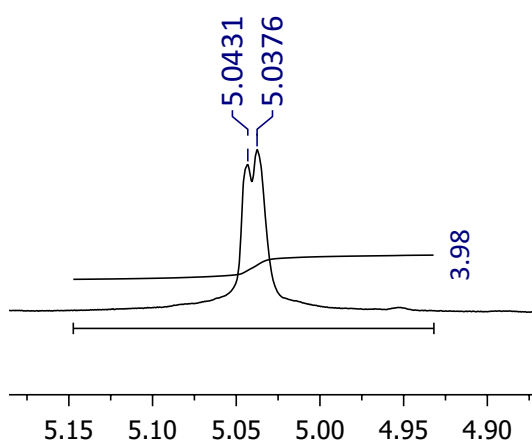
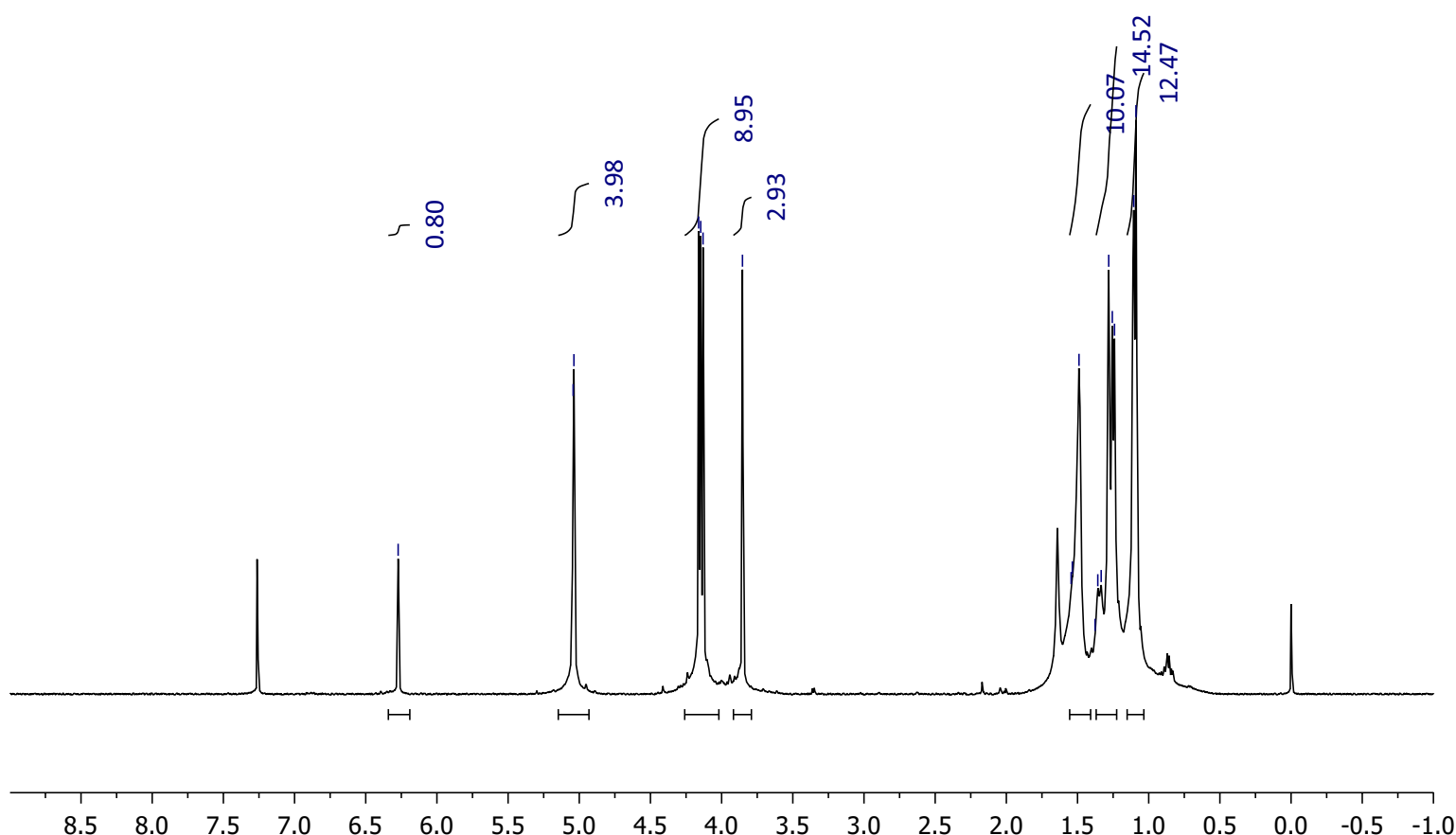
141.0 140.5 140.0

33.5 33.0 32.5

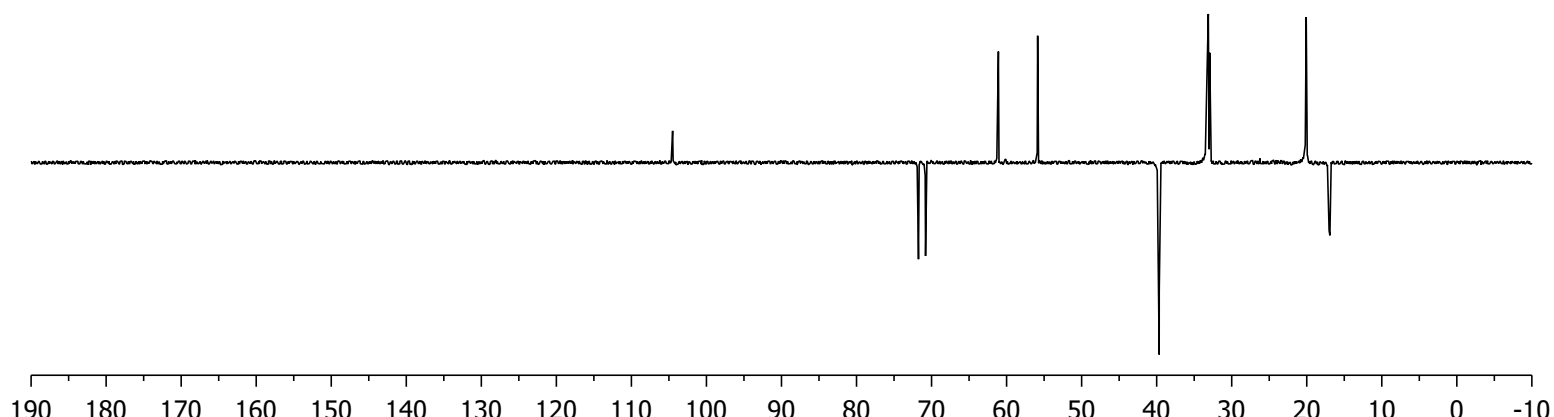
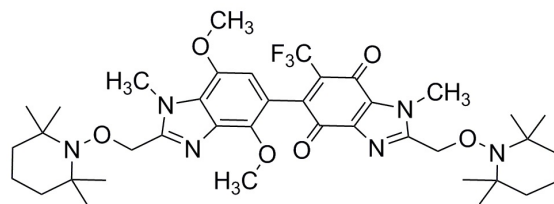
^1H NMR (500 MHz) of **3** in CDCl_3



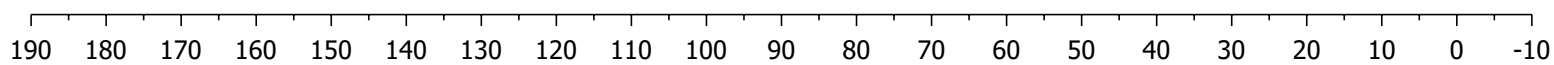
δ 6.2723
 5.0431 5.0376
 4.1615 4.1469 4.1306 3.8536
 1.5450 1.5366 1.4896 1.3766 1.3576 1.3339 1.2810 1.2558 1.2403 1.1054 1.0895



^{13}C NMR (125 MHz) of **3** in CDCl_3



178.1466
174.6264
152.3411
150.1634
147.8489
147.8355
143.1512
142.1119
140.5369
135.4228
131.2391
130.9645
130.7447
130.5245
130.3045
128.7240
125.0616
122.8492
120.6371
118.4241
113.7741
104.5000
71.7425
70.8005
61.0909
60.2016
60.0835
55.8594
39.7202
39.6633
33.2434
33.1161
32.9318
20.0637
17.0192
16.9145



131.2391
130.9645
130.7447
130.5245
130.3045

61.0909
60.2016
60.0835

39.7202
39.6633

33.2434
33.1161
32.9318

17.0192
16.9145

131.4 130.5

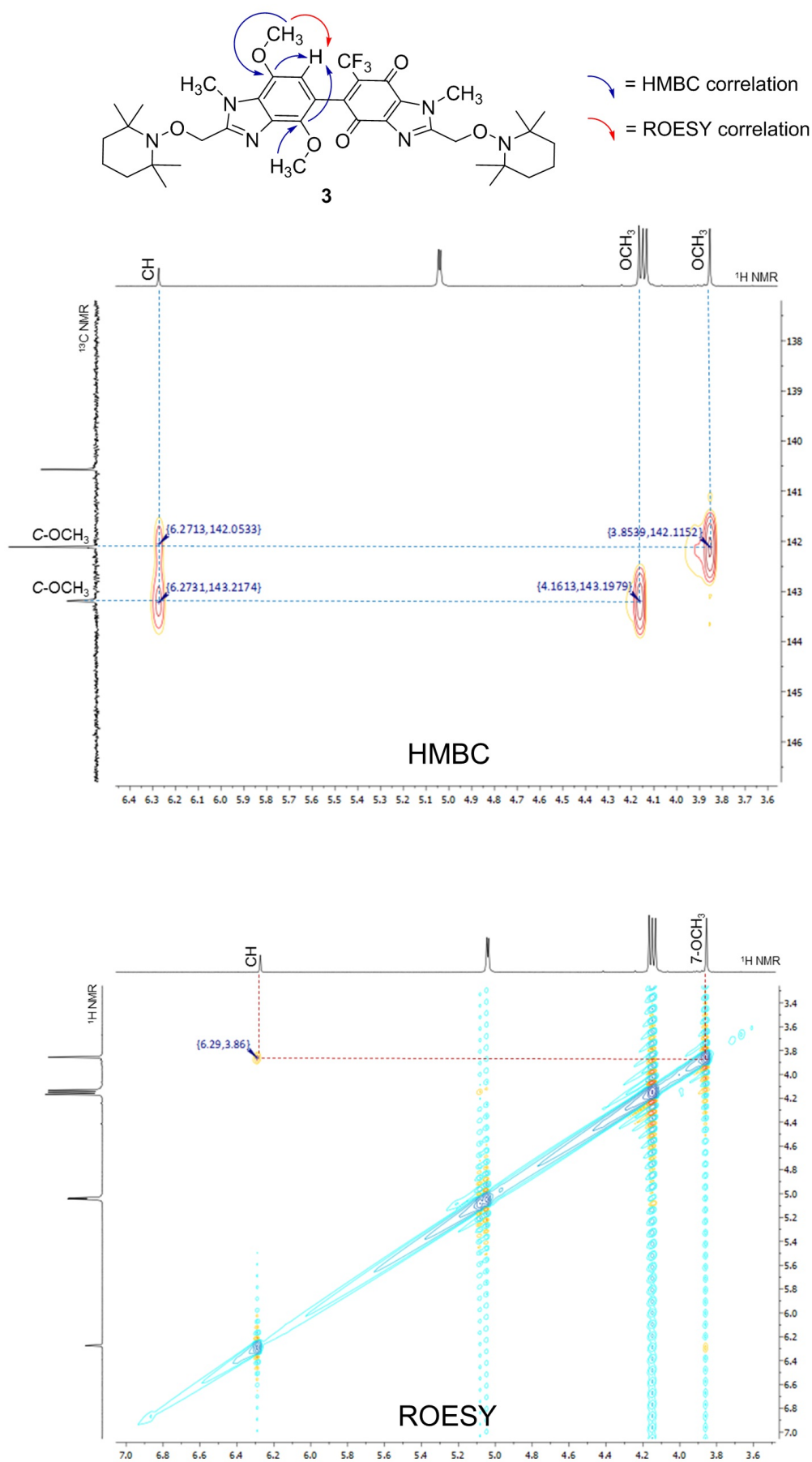
61.2 60.3

40.0 39.6

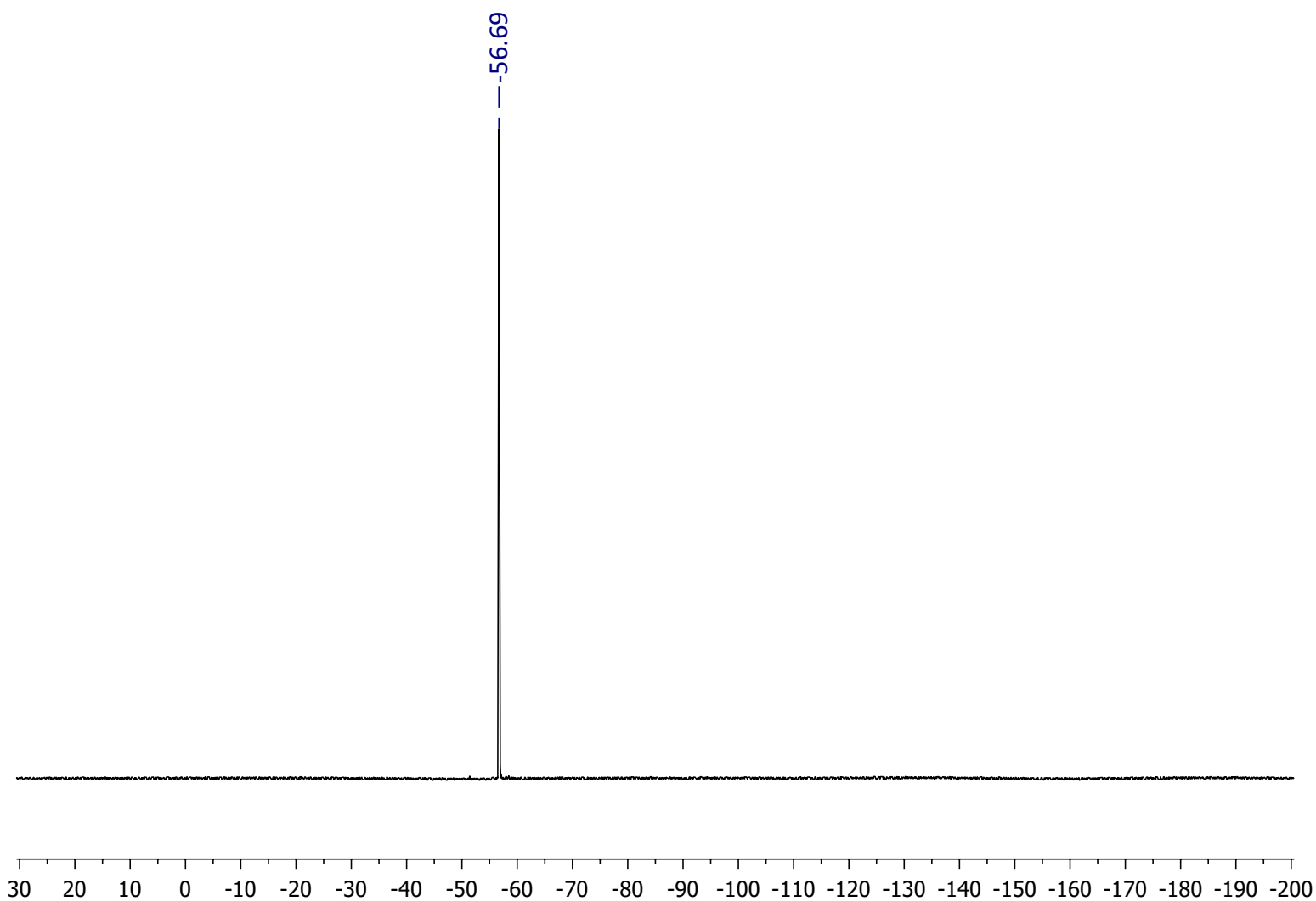
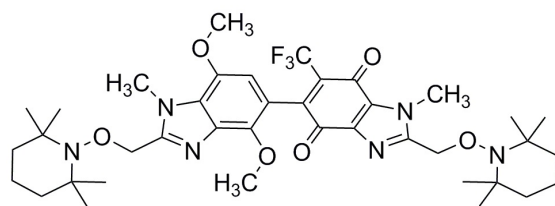
33.3 32.4

17.5 17.0 16.5

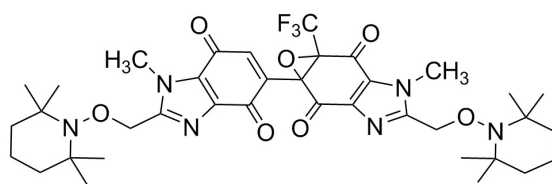
Key HMBC and ROESY couplings in 3



^{19}F NMR (470 MHz) of **3** in CDCl_3



^1H NMR (500 MHz) of **4** in CDCl_3

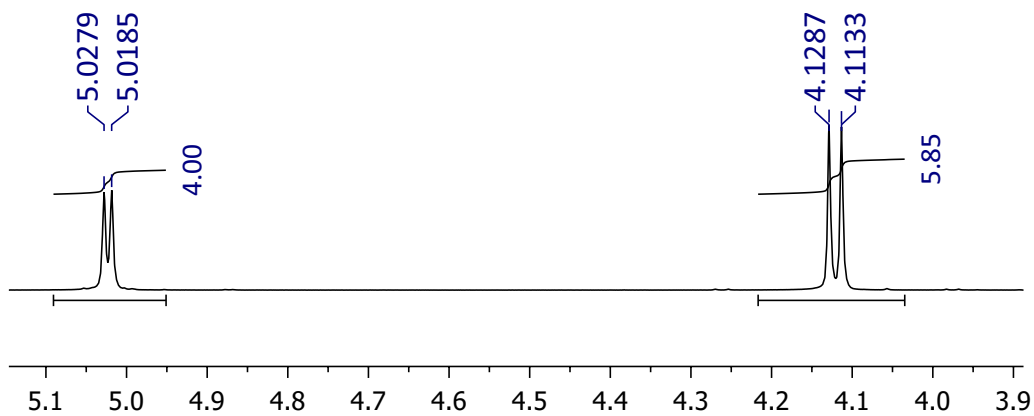
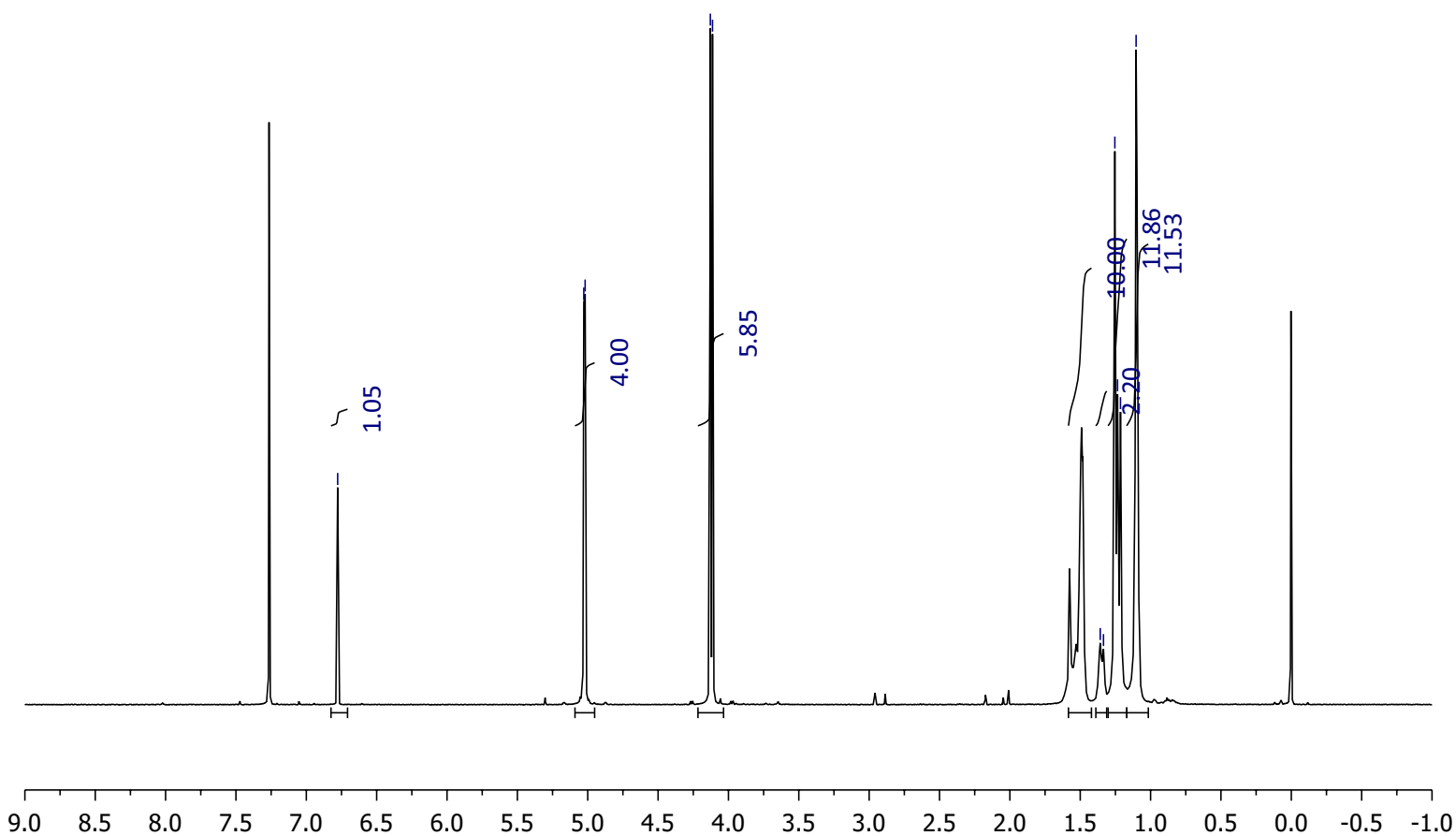


6.7772

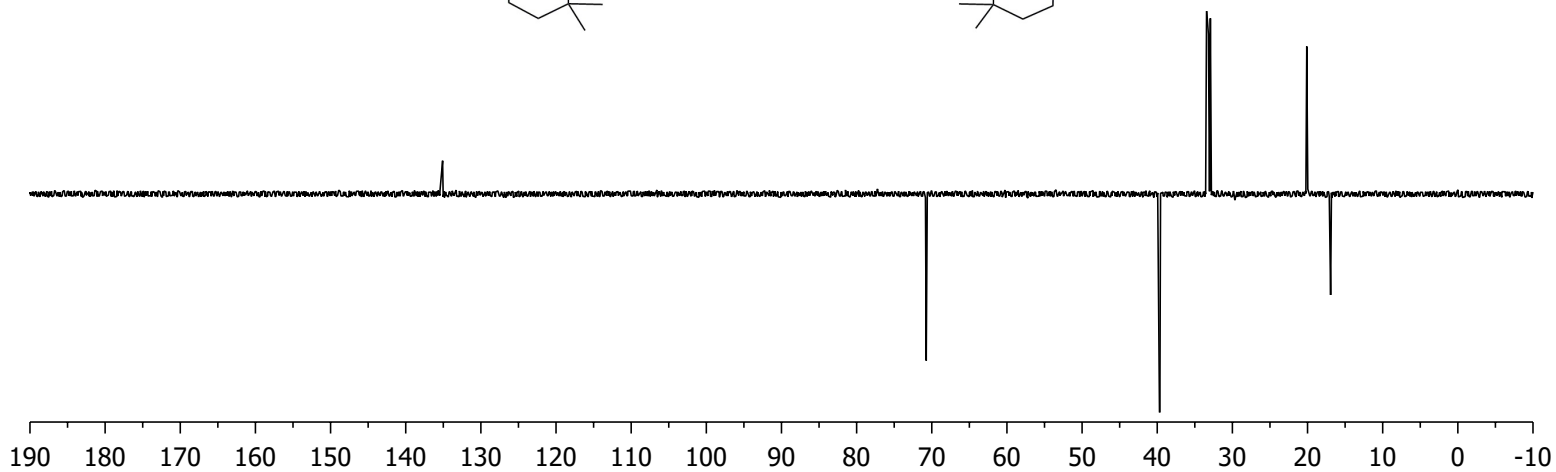
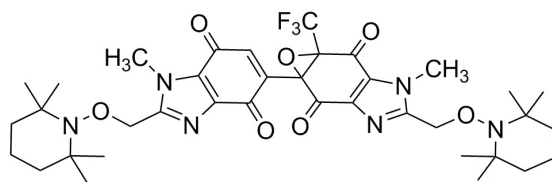
5.0279
5.0185

4.1287
4.1133

1.3578
1.3347
1.2540
1.2349
1.2139
1.1029



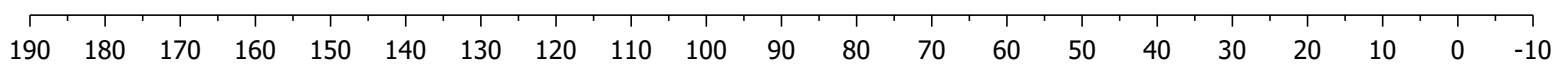
^{13}C NMR (125 MHz) of **4** in CDCl_3



179.5095
178.0775
176.9346
176.1467

154.2098
151.7820
140.3949
140.1846
138.9216
135.0923
132.1549
131.2804
123.8054
121.5593
119.3124
117.0669

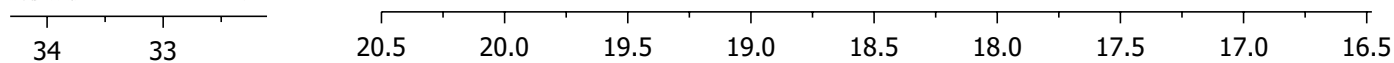
70.7352
70.7187
65.5656
63.7790
63.5082
63.2373
62.9658
60.3204
60.2449
39.6925
39.6704
33.4352
33.2451
33.1921
32.9257
20.1057
20.0824
16.9283
16.9009



33.4352
33.2451
33.1921
32.9257

20.1057
20.0824

16.9283
16.9009



70.7352
70.7187

63.7790
63.5082
63.2373
62.9658

60.3204
60.2449

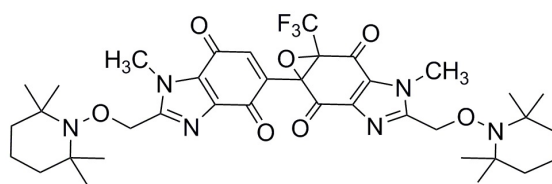
39.6925
39.6704

70.9 70.8 70.7 70.6

64 63 62 61 60

39.9 39.7 39.5

^{19}F NMR (470 MHz) of **4** in CDCl_3



—65.81

